Quantum Monte Carlo study of one-dimensional Bose-Fermi mixtures

Odak, Gloria

Master's thesis / Diplomski rad

2019

Degree Grantor / Ustanova koja je dodijelila akademski / stručni stupanj: **University of Split, University of Split, Faculty of science / Sveučilište u Splitu, Prirodoslovno-matematički fakultet**

Permanent link / Trajna poveznica: https://urn.nsk.hr/urn:nbn:hr:166:253466

University of Split
Faculty of Science

Quantum Monte Carlo study of one-dimensional Bose-Fermi mixtures

Master thesis

Gloria Odak

Split, July 24, 2019

Temeljna dokumentacijska kartica

Sveučilište u Splitu
Prirodoslovno – matematički fakultet
Odjel za fiziku
Ruđera Boškovića 33, 21000 Split, Hrvatska

Diplomski rad

Istraživanje bozonsko fermionskih mješavina metodom kvantnog Monte Carla

Gloria Odak

Sveučilišni diplomski studij Fizika, smjer Računarska fizika

Sažetak:

U radu predstavljamo dobivena svojstva osnovnog stanja jedno-dimenzionalnih fermionskih i bozonsko-fermionsih mješavina s odbojnom kontaktnom interakcijom u vanjskoj harmoničkoj zamci. Mješavine su proučene korištenjem kvantnih Monte Carlo metoda, za koje je u radu razvijen računalni kod, s posebnim fokusom na osobine povezane s energijom i profile gustoće. Podaci dobiveni za fermionske mješavine slažu se s rezultatima iz literature. Zbog osobitosti odbojne interakcije u jednoj dimenziji koja može imitirati kvantnu statistiku, opažena je fermionizacija bozonsko-fermionskih mješavina u sustavu u kojem bozoni međudjeluju odbojno. S druge strane, u sustavu bez interakcije među česticama iste komponente s porastom konstante vezanja opažena je separacija bozonskih i fermionskih komponenti.

Ključne riječi: hladni atomi, 1D mješavine, kvantni Monte Carlo, fermionske mješavine, bozonsko-fermionske mješavine, sustavi u zamci, kontaktna odbojna interakcija, Tanov kontakt, sustavi malog broja čestica

Rad sadrži: 51 stranicu, 18 slika, 0 tablica, 46 literaturnih navoda. Izvornik je na engleskom jeziku.

Mentor: prof. dr. sc. Leandra Vranješ Markić

Ocjenjivači: prof. dr. sc. Leandra Vranješ Markić,
doc. dr. sc. Larisa Zoranić,
doc. dr. sc. Petar Stipanović

Rad prihvaćen: 23. srpnja 2019.

Rad je pohranjen u Knjižnici Prirodoslovno – matematičkog fakulteta, Sveučilišta u Splitu.

Basic documentation card

University of Split
Faculty of Science
Department of Physics
Ruđera Boškovića 33, 21000 Split, Croatia

Master thesis

Quantum Monte Carlo study of one-dimensional Bose-Fermi mixtures

Gloria Odak

University graduate study programme Physics, orientation Computational Physics

Abstract:

We present obtained ground-state properties of one-dimensional Fermi-Fermi and Bose-Fermi mixtures with contact repulsion confined in an external harmonic trap. The systems have been studied using quantum Monte Carlo methods, for which own computer code was developed, with special focus on properties connected with energy and density profiles. The obtained data for Fermi mixtures are consistent with the existing results. Because the repulsive interaction in one-dimension which can mimic quantum statistics, fermionization of the Bose-Fermi mixture is observed in a system with intracomponent Bose-Bose repulsion. On the other hand, in a system with no intra-component interaction one observes the separation of the bosonic and fermionic components when the coupling constant increases.

Keywords: cold atoms, 1D mixtures, quantum Monte Carlo, Fermi-Fermi mixture, Bose-Fermi mixture, trapped systems, contact repulsion, Tan contact, few-body systems

Thesis consists of: 51 pages, 18 figures, 0 tables, 46 references. Original language: English.

Supervisor: Prof. Dr. Leandra Vranješ Markić

Reviewers: Prof. Dr. Leandra Vranješ Markić,
Assist. Prof. Dr. Larisa Zoranić,
Assist. Prof. Dr. Petar Stipanović

Thesis accepted: July 23rd, 2019

Thesis is deposited in the library of the Faculty of Science, University of Split.

Contents

1 Introduction

One-dimensional (1D) systems had long been used as theoretical toy models. Indeed, they are much easier to solve than their three-dimensional counterparts. Ever since Bethe solved the Heisenberg model of ferromagnetism [1], his method, now called the Bethe ansatz (BA), has been used in various many-body models. Even when BA fails[1], incredibly efficient numerical methods exist that allow us to access the system's both ground and excited state properties [2].

Due to their topology, 1D systems show very peculiar properties as there is an interplay between quantum statistics and reduced geometry since strongly repulsive contact interaction can replicate Pauli's exclusion principle. The wavefuction exchange symmetry between identical particles is governed by the spin of the particles, fermions having an antisymmetric wavefunction and bosons a symmetric one. In 1D, all particles are aligned in one line and their exchange is therefore very limited - the only way for two particles to change places is by going through each other. This leads to an enhanced correlation between distinguishable particles and consequentially a failure of many models that are successful in higher dimensions [3, 4].

There is a deep dichotomy between theory and experiment, as far as dimension is concerned. Experimentally, 1D quantum systems are far from simple. They can be realized as condensed matter setups as well as ultracold atomic gases trapped in an external potential limiting the movement of particles to one dimension only. Ultracold atoms are largely tunable which enables experimentalists to search for interaction regimes that are sometimes hard to reach in condensed matter systems [5, 6, 7, 8]. Typically these systems require temperatures as low as a few μK, so in order to achieve effectively 1D regime, very advanced experimental techniques need to be used [9].

In this thesis I will explore the relationship between interaction and statistics in various Fermi and Bose-Fermi mixtures using quantum Monte Carlo methods. The thesis is structured as follows. Chapter 2 is a general introduction into the physics of one-dimensional systems. This includes both very simple models of one and two particles, and some more elaborate models of many-body Bose and Fermi systems. Also, I will give definitions of some relevant quantities and functions. Chapter 3 reviews the quantum Monte Carlo methods that will be used. It contains descriptions of variational and diffusion Monte Carlo algorithms. The details of the implementation are given in Appendix A. The results will be discussed in chapters 4 and 5. Chapter 4 presents a study of ground state properties of various Fermi mixtures and comparison of those results with some published data. Some new results on Bose-Fermi mixtures are given in Chapter 5.

[1] The Bethe ansatz is widely used for many-body quantum systems but it cannot describe the situation we most often encounter experimentally, a system of particles confined in a limited area in space, the so-called trapped systems. All systems I am going to deal with in this thesis will be trapped by an external harmonic potential.

2 Physics in one dimension

Even though we perceive our world as three dimensional and think of lower dimensions as overly simplified models, 1D systems are more than a mere theoretical construct. Recent developments in experiments involving ultracold gases have enabled physicists to explore real-world quantum 1D problems. These effectively 1D systems can be realized by confining atoms in very elongated tight magnetic traps. Their interactions can then be fine-tuned by exploiting Feshbach resonances, creating an opportunity for exploration of fundamental many-body quantum physics [5, 6, 7, 8]. Furthermore, it is possible to mix different kinds of particles of different mass or even particles of the same species tuned to different hyperfine states [10, 11]. Interestingly, the old toy models sometimes capture the properties of the real systems fairly well [12, 13, 14]. However, as it often is in physics, the development of new technology and experimental advancement has caused an outburst of theoretical work in the field [15, 16].

This chapter is organized as follows: first I will give solutions to very simple 1D quantum mechanical problems - two-body scattering and one particle in a harmonic trap. Second, I introduce the concept of correlation functions as useful tools in many-body physics, followed by the definition of Tan's contact as an appropriate tool to characterize 1D systems. And finally, I will very briefly discuss some exactly solvable models of interacting particles, both bosons, and fermions.

2.1 Two body scattering

Let us consider a general two-particle Hamiltonian

$$\hat{H}\left(x_1, x_2\right) = -\frac{\hbar^2}{2m_1}\frac{\partial^2}{\partial x_1^2} - \frac{\hbar^2}{2m_2}\frac{\partial^2}{\partial x_2^2} + \hat{V}\left(|x_1 - x_2|\right)$$

The corresponding Schrödinger equation $\hat{H}\psi = E\psi$ is easily solved by separating the particles' relative movement of that of the center of mass. The wavefunction of the center of mass is simple - it behaves as a free particle of mass $M = m_1 + m_2$. The Hamiltonian of relative motion now takes the form

$$\hat{H}\left(x\right) = -\frac{\hbar^2}{2\mu}\frac{\partial^2}{\partial x^2} + \hat{V}\left(x\right)$$

where $x = |x_1 - x_2|$ is the relative position of particles 1 and 2 and $\mu = \frac{m_1 m_2}{m_1 + m_2}$ is their reduced mass. In this way we have reduced the two-body problem to an effective one-body problem. Since we are going to observe systems with repulsive interactions only, we are here going to consider scattering with positive energy. Now the scattering energy can be written as

$E = \hbar^2 k^2 / (2\mu)$, $k \in \mathbf{R}$. The Schrödinger equation is

$$\frac{d^2}{dx^2}\psi(x) + \left(k^2 - \frac{2\mu \hat{V}(x)}{\hbar^2}\right)\psi(x) = 0$$

and its solution far away from the range of the potential is

$$\psi(x) = sin(kx + \varphi(k)). \tag{2.1}$$

In other words, the interaction only adds a momentum-dependent phase shift to the wavefunction. In the limit of low scattering energy, the details of the potential are no longer relevant and the phase shift depends only on one parameter called the scattering length

$$a_s := -\lim_{k\to 0} \frac{\varphi(k)}{k}. \tag{2.2}$$

The scattering length a_s represents a radius of a hard spherical potential which would reproduce the same phase shift. Namely, this means that for the sake of our calculations, if the incoming particle's momentum is low enough, we can replace whatever the potential really is with another function of the same scattering length. In this thesis I will exploit this fact and use very simple zero range contact pseudo-potential, obtaining the Hamiltonian

$$\hat{H}(x) = -\frac{\hbar^2}{2\mu}\frac{\partial^2}{\partial x^2} + g\delta(x), \tag{2.3}$$

where δ is the Dirac delta function. Now, demanding that (2.1) is an eigenfunction of the Hamiltonian (2.3) we get

$$\varphi(k) = \arctan\frac{\hbar k}{\mu g}$$

and, from the definition (2.2) we get the connection between interaction strength g and the scattering length

$$a_s = -\frac{\hbar^2}{\mu g} \tag{2.4}$$

A more detailed discussion can be found in any quantum mechanics textbook such as [17].

2.2 One particle in a harmonic potential

One dimensional harmonic oscillator is among the first quantum mechanical problems a student encounters in an introductory quantum mechanics course. Here it is covered in order to justify the choice of units for the remainder of the thesis. A more detailed discussion can be found in [17].

Schrödinger equation describing one particle of mass m confined in a one-dimensional har-

monic potential of frequency ω is

$$\left(-\frac{\hbar^2}{2m}\frac{d^2}{dx^2}+\frac{1}{2}m\omega^2x^2\right)\psi\left(x\right)=E\psi\left(x\right)$$

and, with a proper choice of units, can be reduced to

$$\frac{d^2\psi\left(x\right)}{dx^2}+\left(\frac{2mE}{\hbar^2}-\frac{x^2}{a_{osc}^4}\right)\psi\left(x\right)=0,$$

where

$$a_{osc}=\sqrt{\frac{\hbar}{m\omega}} \tag{2.5}$$

is called the oscillator length and will be used as a length unit. We can set $a_{osc}=1$ and omit it from further expressions.

This equation can be solved either analytically or algebraically in a fairly simple way. Here I will only state the solutions. The wavefunction is given as

$$\psi_n\left(x\right)=\left(2^n n!\sqrt{\pi}\right)^{-\frac{1}{2}}e^{-\frac{x^2}{2}}H_n\left(x\right)\qquad n\in\mathbf{Z}_+, \tag{2.6}$$

where $H_n\left(x\right)$ are Hermite polynomials

$$H_n\left(x\right)=\left(-1\right)^n e^{x^2}\frac{d^n}{dx^n}e^{-x^2}.$$

The corresponding energies are

$$E_n=\hbar\omega\left(n+\frac{1}{2}\right)$$

which further simplifies with a choice of energy units $\hbar\omega=1$,

$$E_n=n+\frac{1}{2}$$

These units will be used in most of the thesis since our systems are going to be confined in a trapping potential just like this one.

2.3 Correlation functions

By adding more elements to the system, the particles lose their individuality and become correlated. Correlation functions enable us to explore the properties of the system as a whole, seen as composite of smaller subsystems. Here we define those that will be used later.

Following the pedagogical approach of [18], we start with a general Hamiltonian consisting of one- and two-particle operators.

$$\hat{H} = \hat{F}^{(1)} + \hat{F}^{(2)}$$

The one-particle operator can be expressed as a sum of operators $\hat{f^{(1)}}$ acting on one particle

$$\hat{F}^{(1)} = \sum_i \hat{f}^{(1)}(x_i) \tag{2.7}$$

and similarly,

$$\hat{F}^{(2)} = \sum_{i<j} \hat{f}^{(2)}(x_i, x_j)$$

An example of the one-body operator is an external harmonic potential $V_{ext} = \sum_i \frac{1}{2} m_i \omega^2 x_i^2$, and that of a two-body operator is an internal potential describing the interaction between two particles $V_{int}(x_i, x_j)$. We want to find averages of these operators in order to define density correlation functions. The expected value of (2.7) for an N-particle system is

$$\begin{aligned}
\langle \hat{F}^{(1)} \rangle =& \frac{\int \psi^*(x_1, \ldots, x_N)\, \hat{F}^{(1)}(x_1, \ldots, x_N)\, \psi(x_1, \ldots, x_N)\, dx_1 \cdots dx_N}{\int |\psi(x_1, \ldots, x_N)|^2\, dx_1 \cdots dx_N} \\
=& \frac{\sum_{i=1}^{N} \int \psi^*(x_1, \ldots, x_N)\, \hat{f}^{(1)}(x_i)\, \psi(x_1, \ldots, x_N)\, dx_1 \cdots dx_N}{\int |\psi(x_1, \ldots, x_N)|^2\, dx_1 \cdots dx_N} \\
=& \frac{N \int f^{(1)}(x_1, x_1')\, \psi^*(x_1, \ldots, x_N)\, \psi(x_1', \ldots, x_N)\, dx_1 \cdots dx_N}{\int |\psi(x_1, \ldots, x_N)|^2\, dx_1 \cdots dx_N} \\
=& \iint f^{(1)}(x, x')\, G_1(x, x')\, dx dx',
\end{aligned}$$

where G_1 is the one-body density matrix (OBDM)

$$G_1(x, x') = \frac{N \int \psi(x, \ldots, x_N)\, \psi^*(x', \ldots, x_N)\, dx_2 \cdots dx_N}{\int \psi(x_1, \ldots, x_N)\, \psi^*(x_1, \ldots, x_N)\, dx_1 \cdots dx_N}. \tag{2.8}$$

Here we assumed that the one-particle operator can be both local, like in the case of trapping potential, and non-local, like in the case of kinetic energy, which is why is has two arguments. As for the two-body operator, we take the assumption of locality by default, like in the case of internal potential, so it only has two arguments and not four.

The expression for the two-body density matrix, or the pair correlation function (PCF), is obtained analogously from the average of the two-body operator [18]

$$G_2(x', x'') = \frac{N(N-1) \int |\psi(x', x'', x_3, \ldots, x_N)|^2\, dx_3 \cdots dx_N}{\int |\psi(x_1, \ldots, x_N)|^2\, dx_1 \cdots dx_N}. \tag{2.9}$$

It is often convenient to use dimensionless versions of functions (2.8) and (2.9).

$$g_1(x,x') = \frac{G_1(x,x')}{\sqrt{G_1(x,x)}\sqrt{G_1(x',x')}}$$

$$g_2(x,x') = \frac{G_2(x,x')}{G_1(x,x)\,G_1(x',x')}$$

By taking Fourier transforms of OBDM and PCF one obtains the momentum distribution [18]:

$$n(k) = \frac{1}{2\pi}\iint e^{iks} G_1\left(x+\frac{s}{2}, x-\frac{s}{2}\right) dxds$$

and static structure factor:

$$S(k) = 1 + \frac{1}{N}\iint e^{ik(x_2-x_1)}\left(G_2(x_1,x_2) - n(x_1)\,n(x_2)\right) dx_1 dx_2,$$

respectively.

2.4 Tan's contact

Let us consider a system with contact interactions. Due to the behavior of the many-body wavefunction at short distances which is fixed by the interaction, the momentum distribution in the limit of high momenta displays a universal behavior [19, 20]

$$n(k) \sim \frac{1}{k^4}.$$

It was shown by Tan in 2008 [21, 22, 23] that the weight of the momentum distribution tails C, know as the Tan's contact, is related to the equation of state as

$$C = \frac{dE_0}{da_s}, \tag{2.10}$$

where E_0 is the system's ground state energy and a_s the s-scattering length. Tan's adiabatic theorem, and its 1D version [24], also connect the interaction energy, $E_{int} = \langle g\sum_{i<j}\delta(x_i - x_j)\rangle$ with the contact using Hellman-Feynman theorem as $E_{int} = -a_s dE_0/da_s$, which using (2.10) leads to

$$E_{int} = -a_s C. \tag{2.11}$$

Other than this, Tan's contact provides a number of universal relations connecting short-range correlations with the thermodynamics of the entire system. It has recently been a topic of interest in the field of ultracold gases since the high-momentum region of the momentum distribution can be experimentally accessed [25, 26].

2.5 Models of interacting bosons

A general Hamiltonian describing N bosons of mass m interacting via potential V_{int} in an external potential V_{ext} is given with

$$\hat{H} = \sum_{i=1}^{N} \left[\frac{-\hbar^2}{2m} \frac{\partial^2}{\partial x_i^2} + V_{ext}(x_i) \right] + \sum_{i<j=1}^{N} V_{int}(|x_i - x_j|). \tag{2.12}$$

Expression (2.12) takes the simplest form if we set $V_{ext} = 0$ and $V_{int}(x) = g\delta(x)$ resulting with the following Hamiltonian

$$\hat{H} = \sum_{i=1}^{N} \frac{-\hbar^2}{2m} \frac{\partial^2}{\partial x_i^2} + \sum_{i<j=1}^{N} g\delta(|x_i - x_j|). \tag{2.13}$$

This model was first introduced by Lieb and Liniger in 1963 [27, 28]. They descirbed the interaction via a new parameter $\gamma := mg/\hbar^2$. In the limit $\gamma = 0$ this corresponds to a system of non-interacting bosons. In the so called Tonks-Girardeau (TG) limit ($\gamma \to \infty$) it is a system of impenetrable bosons which can be solved by mapping onto a system of free fermions [29]. Lieb and Liniger showed that the eigenproblem of (2.13) can be solved exactly for every γ using the Bethe ansatz. There is also a generalization of Lieb-Liniger (LL) model with Feshbach-resonant interactions whose approximate solution was also obtained with Bethe ansatz [30].

Lieb-Liniger model is not the only integrable model of 1D bosons. By setting

$$V_{int}(x) = \frac{g}{x^2}$$

either without the external potential $V_{ext} = 0$ or with a harmonic trap $V_{ext}(x) = \frac{1}{2}m\omega^2 x^2$, one obtains another integrable model first introduced by Calogero [31] in 1969. It is characterized by a parameter λ defined with a quadratic equation $\lambda(\lambda - 1) = 2mg/\hbar^2$, the limit $\lambda = 0, 1$ corresponding to TG limit.

Other experimentally relevant types of interaction that are not exactly solvable include

$$V_{int}(x) \sim \frac{1}{|x|^3}$$

which is used to describe dipoles in one dimension. There is also the unscreened Coulomb potential

$$V_{int}(x) \sim \frac{1}{x^2}$$

relevant for charged particles. Some models include external potentials, mostly periodic, trapping or disorder models. Solving a system in a periodic external potential often requires the use of various lattice models. Disorder naturally occurs in condensed matter systems and can

be artificially added to cold atom systems. In one dimensional bosons it sometimes results in a glassy phase of matter. Since ultracold gases need to be contained, trapping potentials are often very important. Experimentally they are realized as magnetic fields or laser lights and are often modeled by a harmonic potential

$$V_{ext}(x) = \frac{m\omega^2 x^2}{2}$$

which is what I am going to use throughout this thesis.

We are now going to briefly consider the solutions of the above-mentioned integrable models. For a more detailed discussion the reader is referred to [3] and references therein.

2.5.1 The Tonks-Girardeau model

As was already mentioned, the TG model is a limit of LL model described with Hamiltonian (2.13) in the limit of infinite repulsion. This type of interaction between particles imposes a constraint that the many-body wavefunction ψ_{TG} must vanish whenever two particles touch. This is also the case for indistinguishable non-interacting spinless fermions. Since they obey Fermi-Dirac statistics, their wavefunction ψ_{FF} is antisymmetric and therefore equal to zero when any two particles meet. Girardeau [29] implemented this constraint in the wavefunction as follows:

$$\psi_{TG}(x_1, \ldots, x_n) = S(x_1, \ldots x_n)\, \psi_{FF}(x_1, \ldots x_n), \tag{2.14}$$

where

$$S(x_1, \ldots, x_n) = \prod_{i>j=1}^{n} \operatorname{sgn}(x_i - x_j) \in \{-1, 1\} \, \forall (x_1, \ldots, x_n)$$

is a function that compensates for the sign change of ψ_{FF}, ensuring proper exchange symmetry of ψ_{TG}. Eigenstates must satisfy the free Schrödinger equation when all n coordinates are different, so on a ring of circumference L with periodic boundary conditions, the ground state wavefunction has the form

$$\psi_{TG}(x_1, \ldots, x_n) = \sqrt{\frac{2^{n(n-1)}}{n! L^n}} \prod_{i>j=1}^{n} \left| \sin\left[\frac{\pi}{L}(x_i - x_j)\right] \right| \tag{2.15}$$

This wavefunction is actually generic of many 1D models in the limit of infinite repulsion, including both the Lieb-Liniger and the Calogero model [3]. The ground state energy in the thermodynamic limit is given with [3]

$$E_{TG} = \frac{\hbar^2 \pi n^2}{6mL^2}$$

The Bose-Fermi mapping (2.14) is also valid in the presence of an external trapping potential V_{ext}. The eigenstates are then constructed as Slater determinants of the non-interacting trapped

Hamiltonian. In the case of harmonic confining potential, the eigenfunctions are given with (2.6) which yields the many-particle wavefunction [32]

$$\psi_{TG}\left(x_1,\ldots,x_n\right)=\sqrt{C_n}\prod_{k=1}^{n}e^{\frac{-x_k^2}{2}}\prod_{i<j=1}^{n}\left|x_i-x_j\right|,$$

where $C_n=n!\prod_{m=0}^{n-1}2^{-m}\sqrt{\pi}m!$. It was shown in [32] that density profile for TG gas is the same as in the case of free spinless fermions, but the off-diagonal correlations as well as the momentum distributions differ in both homogeneous and trapped case.

2.5.2 The Lieb-Liniger model

The more general LL model 2.13 is integrable [28, 27] with the ansatz

$$\psi_{LL}=\sum_{\sigma\in S_n}A\left(\sigma\right)e^{i\sum_m k_{\sigma(m)}x_m}, \tag{2.16}$$

where k_i is the pseudo-momentum[2] of the ith boson, and A is a function that takes interaction into account and depends on the ordering of the particles, we take $x_1<x_2<\cdots<x_n$ and S_n is the symmetric group of permutations of the set $\{1,2,\cdots,n\}$. The value of (2.16) when the ordering $x_1<x_2<\cdots<x_n$ is not satisfied follows from the exchange symmetry of the wavefunction.

Now, when all particles' coordinates are different, there is no interaction and the Hamiltonian (2.13) reduces to the Hamiltonian of n free particles whose eigenfunctions are linear combinations of plane waves. If a collision occurs, since we are in 1D regime and we must obey the conservation laws, there are only two possibilities for the colliding particles - each can either emerge from the collision with the same momentum it had before, or the two can exchange momenta. This justifies the use of permutations in the ansatz (2.16) which can be seen as a generalization of the TG wavefunction (2.15), where the nodes of ψ_{TG} are replaced by a more complicated boundary conditions on ψ_{LL}.

A detailed justification and a rigorous proof of the use of the Bethe ansatz can be found in [33] and a comprehensive derivation of the LL wave function is given in chapter 3 of [34].

Here I will only state their results. In the units where $\hbar^2/\left(2m\right)=1$ the wavefunction for a finite number of bosons is given with

$$\psi_{LL}\left(x_1,\ldots,x_n\right)=\frac{\prod_{j>i=1}^{n}\left(k_j-k_i\right)}{\sqrt{n!\prod_{j>i=1}^{n}\left[\left(k_j-k_i\right)^2+g^2\right]}}\sum_{\sigma\in S_n}\prod_{j>i=1}^{n}\left[1-\frac{ig\mathrm{sgn}\left(x_j-x_i\right)}{k_{\sigma(j)}-k_{\sigma(i)}}\right]\prod_{j=1}^{n}e^{ik_jx_j}$$

[2]The prefix *pseudo* comes from the fact that the ks are not observable and should not be confused with physical momenta.

and the corresponding ground state energy is

$$E_0 = \sum_{i=1}^{n} k_i^2.$$

In the thermodynamic limit, letting the number of particles and the size of the system grow $N, L \to \infty$ while keeping the density $n = N/L$ finite, the system of infinitely many Bethe ansatz equations boils down to a set of three integral equations yielding the expression for the ground state energy

$$\frac{E_0(\gamma)}{N} = \frac{\hbar^2}{2m} n^2 e(\gamma) \tag{2.17}$$

where $e(\gamma)$ is a dimensionless function of the strength of the interaction $\gamma = mg/(\hbar^2 n)$.[3] The function e and the energy (2.17) are obtained by solving the system of equations

$$\begin{aligned} g_\lambda(x) &= \frac{1}{2\pi} + \frac{1}{\pi} \int_{-1}^{1} g_\lambda(y) \frac{\lambda}{\lambda^2 + (x-y)^2} dy \\ \gamma &= \lambda \left(\int_{-1}^{1} g_\lambda(x) dx \right)^{-1} \\ e(\gamma) &= \frac{\gamma^3}{\lambda^3} \int_{-1}^{1} g_\lambda(x) x^2 dx \end{aligned}$$

which is not integrable but can be solved numerically.

2.6 Models of interacting fermions

After the development of the LL model, a lot of effort was put into solving the same Hamiltonian but for a system of identical spin-$\frac{1}{2}$ fermions.

$$\hat{H} = \sum_{s=\uparrow\downarrow} \sum_{i=1}^{N} \frac{-\hbar^2}{2m} \frac{\partial^2}{\partial x_i^{s2}} + \sum_{i,j=1}^{N} g\delta\left(\left| x_i^{\uparrow} - x_j^{\downarrow} \right| \right). \tag{2.18}$$

Here we omit the interaction terms between the same spin particles since exchange symmetry of the wavefunction ensures the particles are never in the same place. The Hamiltonian (2.18) was solved by Yang and Gaudin using the Bethe ansatz [35, 36]. Even though the Yang-Gaudin (YG) model is most often mentioned with spin-$\frac{1}{2}$ fermions in mind, [35] gives a solution for contact interaction Hamiltonian (2.13) in any irreducible representation of the group S_N of permutation of the coordinates and is therefore valid for both bosons and fermions of any spin.

[3] Notice that the linear density n appears in the denominator of the interaction strength γ. This is very counter-intuitive, it means that by diluting the system, the interaction strength increases. This means that the TG regime $\gamma \to \infty$ actually corresponds to very dilute gases, $n \to 0$.

The ansatz is given with

$$\psi = \sum_{\sigma,\tau \in S_N} A\left(\sigma,\tau\right) e^{i\sum_{j=1}^{N} k_{\sigma(j)} x_{\tau(j)}}$$

where both σ and τ are permutations of the coordinates and the sum goes over $N! \times N!$ terms. Here I will list the integral Bethe ansatz equations for the case of repulsive interactions $g > 0$ in the thermodynamic limit. For the derivation and a more detailed discussion see [4].

$$\begin{aligned}
p_1 &= \frac{1}{2\pi} + \int_{-A_2}^{A_2} K_1\left(k-k'\right) p_2\left(k'\right) dk' \\
p_2 &= \int_{-A_1}^{A_1} K_1\left(k-k'\right) p_1\left(k'\right) dk' - \int_{-A_2}^{A_2} K_2\left(k-k'\right) p_2\left(k'\right) dk' \\
K_l(x) &= \frac{1}{2\pi} \frac{lc}{(lc/2)^2 + x^2}
\end{aligned}$$

where the integration boundaries are determined from the conditions

$$\begin{aligned}
\frac{N}{L} &= \int_{-A_1}^{A_1} p_1(k) dk \\
\frac{N_\downarrow}{L} &= \int_{-A_2}^{A_2} p_2(k) dk \\
\frac{E}{L} &= \int_{-A_1}^{A_1} k^2 p_1(k) dk.
\end{aligned}$$

3 Quantum Monte Carlo

Monte Carlo methods encompass a broad class of algorithms whose common characteristic is the use of random numbers for solving problems that might be deterministic in principle. They are widely used for finding solutions of non-integrable or otherwise difficult problems.

Quantum Monte Carlo (QMC) methods are powerful tools which allow treatment and description of the many-body effects encoded in the wavefunction. In this thesis I am going to use two flavors of QMC. The core method is the Diffusion Monte Carlo (DMC), which is exact for calculations of the ground state of a Bose system. Its modification for fermions, the Fixed-Node Diffusion Monte Carlo (FN-DMC) gives an upper bound of the ground state energy but with a good choice of the trial wavefuncton can be a very accurate approximation. The Variational Monte Carlo (VMC) is based on the variational principle of quantum mechanics and is used for optimization of the wavefunction before doing DMC and FN-DMC.

Mathematically, the core of every Monte Carlo method is the theory of Markov processes, which is why I start this chapter with the definition of a Markov chain. Secondly, I introduce the techniques of importance sampling, first generally and then by giving a specific example used in QMC methods here - the Metropolis algorithm. After that I am going to discuss variational principle and its implementation through VMC. Finally, I will describe the theory behind DMC for bosons and FN-DMC for fermions.

This chapter will contain the theoretical overview of these methods. For the most part I will follow the approach of Thijssen's chapters 10 and 12 [2]. The pseudocode and examples of the source code will be omitted here and instead be given in larger detail in Appendix A.

3.1 Markov chains

A Markov chain is a series of stochastic events in which the probability of each events depends only on the previous state and not the entire chain. This property is sometimes calles *memorylessness*, for obvious reasons. To better understand Markov chains, we first consider an uncorrelated chain. The probability of occurence of a series of events $\{x_1, \ldots, x_N\}$ is statistically uncorrelated if

$$P_N(x_1, \ldots, x_N) = P(x_1) \cdots P(x_N),$$

where $P(x)$ is the probability of occurrence of the event x and is assumed to be equal for each step. From the definition of a Markov chain, we see that the probability $P_N(x_1, \ldots, x_N)$ will have to contain transition probabilities $T(x_i \to x_j)$ for event x_j happening right after event x_i.

The probability for having a sequence $(x_1, \ldots, x_N)$[4] then becomes

$$P_N(x_1, \ldots, x_N) = P(x_1)\, T(x_1 \to x_2) \cdots T(x_{N-1} \to x_N)$$

A Markov chain is ergodic if it satisfies the following two properties [2]:

- the chain is connected - any configuration is accessible from any other configuration in a finite number of steps
- the chain is not periodic - a realized configuration must not be realized again after a fixed number of steps

These conditions ensure that after sufficiently long time, the entire phase space will be covered. Let p be a probability distribution function such that $p(X,t)$ is a probability of configuration X occurring in a Markov step t. From step to step, the change in p is governed by two processes described by the *master equation* [2]:

$$p(X,t+1) - p(X,t) = -\sum_{X'} T(X \to X')\, p(X,t) + \sum_{X'} T(X' \to X)\, p(X',t) \tag{3.1}$$

which describes the transition from X to any new configuration and the transition to X from any old configuration. We are interested in finding a stationary distribution so that (3.1) equals zero, i.e. $p(X,t+1) = p(X,t)$. Even though finding a general solution for

$$\sum_{X'} T(X \to X')\, p(X,t) = \sum_{X'} T(X' \to X)\, p(X',t)$$

is not simple, a sufficient condition for a Markov process to be stationary is obvious

$$T(X \to X')\, p(X,t) = T(X' \to X)\, p(X',t), \quad \forall X, X'. \tag{3.2}$$

This defines the *detailed balance* condition.

3.2 Importance sampling

A simple application of Monte Carlo is the evaluation of a definite integral

$$F = \int_a^b f(x)\, dx. \tag{3.3}$$

[4] Here I use different parentheses on purpose, to emphasize the fact that events in a Markov chain are ordered, contrary to those in an uncorrelated chain.

Using the mean value theorem,

$$F = (b-a) \lim_{n\to\infty} \frac{1}{n} \sum_{i=1}^{n} f(x_i),$$

where $x_i = a + i(b-a)/n$ for a given n. Of course, to evaluate this numerically, a cut-off needs to be made for a finite n.

$$F_n = (b-a) \frac{1}{n} \sum_{i=1}^{n} f(x_i), \tag{3.4}$$

We can further expand this as

$$F_n = (b-a) \frac{\sum_{i=1}^{n} \omega_i f(x_i)}{\sum_{i=1}^{n} \omega_i}, \tag{3.5}$$

where coefficients ω_i are introduced into the sum as weights. This is the starting point for conventional methods of numerical integration which use equidistant (3.4) or otherwise predetermined points (3.5) to sample the function. These algorithms are effective for low-dimensional integrals, but the computational cost of d-dimensional integral evaluation increases as n^d. Since multi-dimensional integration is often unavoidable, more effective methods are needed.
If the points $x_i \in [a,b]$ are chosen at random, by the central limit theorem, the set of all possible sums over different $\{x_i\}_{i=1}^{n}$ will have a normal distribution and the measure of the uncertainty in the integral's value is the standard deviation

$$\sigma_n = \sqrt{\frac{\frac{b-a}{n} \sum_{i=1}^{n} f^2(x_i) - F_n^2}{n-1}}$$

which decays as $n^{-\frac{1}{2}}$ independent of the dimension of the integral, making Monte Carlo integration very appropriate for calculations in statistical physics and quantum mechanics.

Obviously, the choice of the probability distribution from which to sample the configuration can have a strong impact on the efficiency of the calculation. The simplest approach would be to use the uniform distribution. However, it is often ineffective since not all states contribute to the integral equally, while many functions have significant weight in only a few regions. In order to overcome this problem and increase the overall efficiency, techniques of importance sampling are introduced. These methods consist of sampling from a non-uniform distribution ω chosen carefully to approximate f on the interval $[a,b]$. Now the integral (3.3) can be evaluated by selecting points from the probability distribution p given with

$$p(x) = \frac{\omega(x)}{\int_a^b \omega(x)\, dx},$$

leading to

$$F = \int_a^b f(x)\,dx = \int_a^b \left[\frac{f(x)}{p(x)}\right] p(x)\,dx,$$

where the set $\{x_i\}$ is sampled according to p, and F_n becomes

$$F_n = \frac{1}{n}\sum_{i=1}^{n} \frac{f(x_i)}{p(x_i)}$$

3.3 Metropolis algorithm

In 1953, Metropolis *et al.* published a paper [37] that is considered by many the beginning of modern Monte Carlo methods. They described sampling of the given function as a *random walk* of a mathematical object called *a walker*. The movement of the walker through the state space completely determines the properties of the system. The collection of the walker's movements is called *a chain*. Mathematically this is a Markov chain and the goal is to sample its stationary distribution. In order to construct the algorithm, the transition probability $T(X \to X')$ can be decomposed as

$$T(X \to X') = \omega(X, X')\, A(X, X'),$$

where ω is the trial step probability and A is the acceptance probability. In principle, ω is arbitrary and A is chosen so that it satisfies the detailed balance condition (3.2)

$$A(X, X') = min\left(1, \frac{p(X')\,\omega(X', X)}{p(X)\,\omega(X, X')}\right), \tag{3.6}$$

where all the functions are evaluated in the same Markov step so I use $p(X, t) =: p(X)$. This choice of the acceptance probability ensures sampling according to the targeted distribution p for any choice of ω. To further simplify (3.6), let ω be the Gaussian distribution. Since it is symmetric, $\omega(X, X') = \omega(X', X)$, and

$$A(X, X') = min\left(1, \frac{p(X')}{p(X)}\right),$$

Because of its probabilistic interpretation, for all QMC applications of the Metropolis algorithm, the probability distribution p is the square of the system's wavefunction $|\psi|^2$.

The variance will not affect the equilibrium distribution but it does affect the efficiency of the sampling. A large variance will explore more configurations but that will result in longer simulations since many moves will be rejected. A small variance, on the other hand, means high acceptance rate but the state space is explored very slowly. For an efficient simulation variance will need to be adjusted in order to keep the acceptance rate around 50%. The pseudocode for Metropolis acceptance is given in Appendix A.3.1, algorithm 1, and the scheme for acceptance adjusting is given in listing 4.

3.4 Variational Monte Carlo

The key idea behind the VMC is to use a trial wavefunction $\psi_T(\alpha)$, with free parameters α, and the variational principle of quantum mechanics according to which ψ_T gives an upper bound on the ground state energy

$$E_T = \frac{\langle\psi_T|\hat{H}|\psi_T\rangle}{\langle\psi_T|\psi_T\rangle} \geq E_0. \tag{3.7}$$

By minimizing the variational energy with respect to the variational parameters α, the trial wavefunction approaches the real ground state function. From now on I will assume that the trial wavefunction is normalised, i.e. $\langle\psi_T|\psi_T\rangle = 1$, so the expression (3.7) can be expanded in the coordinate representation as

$$\begin{aligned} E_T &= \int \psi_T*(X)\,\hat{H}\psi_T(X)\,\frac{\psi_T(X)}{\psi_T(X)}dX \\ &= \int \psi_T*(X)\,\psi_T(X)\,\frac{\hat{H}\psi_T(X)}{\psi_T(X)}dX \\ &= \int \psi_T*(X)\,\psi_T(X)\,E_L(X)\,dX, \end{aligned} \tag{3.8}$$

where $E_L(X) := \frac{\hat{H}\psi(X)}{\psi(X)}$ is the *local energy* of the configuration $X = (x_1, \ldots, x_N)$. The integral (3.8) is suitable for Metropolis integration, therefore the energy E_T is calculated as an average local energy E_L sampled according to $|\psi_T|^2$.
The details of the implementation are given in Appendix A.3.1.

3.5 Diffusion Monte Carlo

The DMC method is a Green's function based method for solving the ground state of the Schrödinger's equation. It provides an exact (in statistical sense) solution for the ground state energy. A general N-body system's time evolution is described with the following Hamiltonian

$$\hat{H} = -\sum_{i=1}^{N}\frac{\hbar^2}{2m}\frac{\partial^2}{\partial x_i^2} + \sum_{i<j=1}^{N} V_{int}(x_{ij}) + \sum_{i=1}^{N} V_{ext}(x_i),$$

where $x_{ij} = |x_i - x_j|$ is the distance of particles i and j, V_{int} describes the interactions between particles and V_{ext} is the external potential. An arbitrary state of the system $|\psi\rangle$ can be expanded in the basis of the eigenstates of the Hamiltonian $\{\phi_n\}$ as

$$|\psi(X,t)\rangle = \sum_n c_n\,|\phi_n(X,t)\rangle, \tag{3.9}$$

where $X = (x_1, \ldots, x_N)$. Instead of considering time-evolution, the ground state properties can be investigated by performing a Wick's rotation of the Schrödinger's equation, $it/\hbar \to \tau$,

and evolving the state (3.9) in imaginary time τ according to the equation

$$-\frac{\partial}{\partial\tau}\psi\left(X,\tau\right)=\left(\hat{H}-E_R\right)\psi\left(X,\tau\right),$$

where we introduced a referent energy E_R whose effect is going to become evident later. The evolution of the state (3.9) can be described by the imaginary time propagator

$$\left|\psi\left(X,\tau\right)\right\rangle=\sum_n c_n e^{-\left(\hat{H}-E_R\right)\tau}\left|\phi_n\left(X,0\right)\right\rangle.$$

In a sufficiently long simulation, the contribution of all states with energies larger than E_R exponentially decays. With a good choice of the referent energy $E_R \approx E_0$, the system will evolve to the ground state ϕ_0, independent of the choice of the initial state ψ, as long as they are not orthogonal $\langle\phi|\psi\rangle \neq 0$.

In order to reduce statistical fluctuations, we introduce importance sampling by defining a new distribution

$$\Psi(X,\tau)=\psi_T(X)\psi(X,\tau),$$

where ψ_T is the VMC-optimized wavefunction.

$$-\partial_\tau\Psi(X,\tau)=-D\nabla^2\Psi(X,\tau)+D\nabla\left[F(X)\Psi(X,\tau)\right]+\left[E_L(X)-E_R\right]\Psi(X,\tau), \tag{3.10}$$

where $D:=\hbar^2/(2m)$, $\nabla=\sum_i\partial_i$, and standard abbreviated notation is used for the derivatives; E_L is the local energy defined in (3.8) and a new quantity is introduced, the quantum force F, defined as

$$F(X)=2\frac{\nabla\psi_T}{\psi_T}. \tag{3.11}$$

Notice that the equation (3.10) has the following form:

$$-\partial_\tau\Psi=(\hat{A}_1+\hat{A}_2+\hat{A}_3)\Psi$$

The operators $\hat{A}_i,\ i=1,2,3$, are associated with diffusion, drift and decay processes, respectively. Equation (3.10) is solved using the Green's function method

$$\Psi\left(X',\tau+\triangle\tau\right)=\int G\left(X',X,\triangle\tau\right)\Psi\left(X,\tau\right)dX,$$

where

$$G\left(X',X,\triangle\tau\right)=\langle X'|e^{-\left(\hat{A}_1+\hat{A}_2+\hat{A}_3\right)\triangle\tau}|X\rangle.$$

We can calculate the Green's function independently for each of the operators $\hat{A}_i$. Since they don't commute, the Green's function for their sum cannot be found exactly, but within the

short time approximation, and propagating for a large number of steps, according to Lie-Trotter product formula [38], and the Baker–Campbell–Hausdorff formula [39],

$$e^{-\left(\hat{A}_1+\hat{A}_2+\hat{A}_3\right)\triangle\tau} = e^{-\hat{A}_3\triangle\tau/2}e^{-\hat{A}_2\triangle\tau/2}e^{-\hat{A}_1\triangle\tau}e^{-\hat{A}_2\triangle\tau/2}e^{-\hat{A}_3\triangle\tau/2} + \mathscr{O}(\triangle\tau^3),$$

so

$$\Psi\left(X',\tau+\triangle\tau\right) = \int G_3\left(X',X_1,\frac{\triangle\tau}{2}\right)G_2\left(X_1,X_2,\frac{\triangle\tau}{2}\right)G_1\left(X_2,X_3,\triangle\tau\right)$$
$$G_2\left(X_3,X_4,\frac{\triangle\tau}{2}\right)G_3\left(X_4,X,\frac{\triangle\tau}{2}\right)\Psi\left(X,\tau\right)dX_1dX_2dX_3dX_4dX$$

Analytical solutions to these Green functions are [40]:

$$G_1(X',X,\tau) = \left(\frac{2\pi\hbar^2\tau}{m}\right)^{-\frac{3N}{2}} e^{-\frac{m(X'-X)^2}{2\hbar\tau}}$$
$$G_2(X',X,\tau) = \delta\left(X'-X\left(\tau\right)\right), \text{where } X(0)=X \text{ and } \frac{dX}{d\tau} = \frac{\hbar^2}{2m}F(X)$$
$$G_3(X',X,\tau) = e^{-(E_L(X)-E_R)}\delta\left(X'-X\right).$$

The calculation of the local energy (3.8) can be optimized by separating the Hamiltonian on the kinetic and potential part. The kinetic part of the local energy of the i-th particle is given as

$$E_L^i(x_i) = -D_i\left(\frac{1}{2}\partial_i F_i + \frac{1}{4}F_i\cdot F_i\right), \tag{3.12}$$

where F_i is the drift force acting on the ith particle, and the total energy of the system is

$$E(X) = \sum_{i=1}^{N} E_L^i(x_i) + V_{ext}(X)$$

The details of implementation of DMC are given in Appendix A.3.2.

3.5.1 Fixed Node Diffusion Monte Carlo

The FN-DMC is a modification of the DMC algorithm which allows approximate treatment of a system whose wavefunction has nodes. This includes both the ground state of fermionic systems and excited states of various many-body systems. The distribution of walkers at the end of a DMC simulation corresponds to $\psi(X) = \psi_T(X)\phi_0(X)$. To ensure positive definiteness of ψ, the nodal hypersurfaces of ψ_T and ϕ_0 must match, i.e. they have to change signs together. Since the exact expression for ϕ_0 is not *a priori* know, the nodes of the trial wavefunction ψ_T are fixed by accepting only the moves for which the sign remains unchanged, $\frac{\psi_T(X')}{\psi_T(X)} > 0$, with X and X' representing the old and new configurations, respectively. Due to the nodal constraint, this method only gives an upper bound of the energy, and is as accurate as the guess on the nodal surfaces. Namely, if the nodes of ψ_T were exact, then ψ would be exact.

4 Fermi mixtures

In this chapter I use FN-DMC technique to study the ground state properties of various multi-component fermionic systems. The proper statistics will be imposed by using an antisymmetric trial wavefunction. If the nodes of the trial wave function are exact, the method will yield exact ground state properties, as was described in 3.5.1. Since 1D fermionic wavefunction must vanish when two identical fermions coincide, its nodes are known and the obtained properties are expected to be statistically exact.

I will first define the Hamiltonian and the trial wavefunction that will be used. Then I discuss the results, first the energy and Tan's contact, and then the density profiles. Since some results for 1D fermionic mixtures were already published [41, 42], I will be comparing my results with theirs throughout this chapter so it can be understood as a sort of a test of the code before we continue to the next chapter where some new results will be given.

4.1 Model Hamiltonian and trial wave function

We consider a 1D Fermi gas with contact interaction trapped in a harmonic external potential with frequency ω. The system consisting of N_c components with component α containing N_α particles of equal mass m is described by the Hamiltonian

$$\hat{H} = -\frac{\hbar^2}{2m}\sum_{\alpha=1}^{N_c}\sum_{i=1}^{N_\alpha}\partial_{\alpha i}^2 + g\sum_{\alpha<\beta=1}^{N_c}\sum_{i=1}^{N_\alpha}\sum_{j=1}^{N_\beta}\delta\left(x_i^\alpha - x_j^\beta\right) + \frac{m\omega^2}{2}\sum_{\alpha=1}^{N_c}\sum_{i=1}^{N_\alpha}(x_i^\alpha)^2 \tag{4.1}$$

where $\partial_{\alpha i} = \frac{\partial}{\partial x_i^\alpha}$ and g is a coupling constant which can be fine tuned with Feshbach and Olshanii resonances [43, 44]. The total number of particles is $N = \sum_{\alpha=1}^{N_c} N_\alpha$. The Hamiltonian (4.1) was used in [41] for two-component systems $N = N_1 + N_2$ in balanced $N_1 = N_2$ and slightly imbalanced case $N_2 = N_1 + 1$. Multi-component systems with N_p particles of each component, where $N = N_c N_p$, were considered in [42]. Both cases will be studied here.

The trap imposes a length scale a_{osc}, defined with (2.5), which we use as a length unit. The energy unit will be the $g = 0$ level separation $\hbar\omega$. Another important length scale, the scattering length a_s given with (2.4), is related to particle interaction and depends on the coupling constant g. We will use both a_s and g interchangeably to characterize interaction strength. In order to compare our results with the published data [42], we are also going to use another interaction parameter describing the interaction strength [45], defined with Na_s^2/a_{osc}^2.

The system's behavior in the limits $a_s \to \infty$ and $a_s \to 0$ is known. The former corresponds to $g \to 0$. The system separates to N_c subsystems with subsystem α consisting of N_α non-

interacting indistinguishable fermions in a harmonic trap. The wavefunction is a product of Slater determinants of the harmonic oscillator wavefunctions and the energy is a sum of energies of the subsystems given with $E_\alpha = \sum_{n=0}^{N_\alpha - 1} \left(n + \frac{1}{2}\right)$. The latter corresponds to $g \to \infty$. We already discussed in the section 2.5.1 about the TG model, how this limit was solved for bosons with infinite contact repulsion using the process of fermionization. There is no reason for this not to also apply in the case of distinguishable fermions [7] since the Hamiltonian (4.1) is spin independent. Therefore, we can expect the system with infinite repulsion to behave like the system of $N = \sum_{\alpha=1}^{N_c} N_\alpha$ identical fermions.

The trial wavefunction is constructed in the manner of [42] as a product of correlation terms and Slater determinants $\det S$ of a single-component Fermi gas which ensure the anti symmetry of the fermionic wavefunction

$$\psi_F = \prod_{\alpha=1}^{N_c} \det S\left(X_\alpha\right) \times \prod_{\alpha<\beta=1}^{N_c} \prod_{i=1}^{N_\alpha} \prod_{j=1}^{N_\beta} \left| \left| x_i^\alpha - x_j^\beta \right| - a_s \right|, \tag{4.2}$$

where $X_\alpha = \left(x_1^\alpha, ..., x_{N_\alpha}^\alpha\right)$ is an N_α-dimensional vector that contains the positions of the particles of component N_α. The Slater determinant contains Hermite polynomials and its calculation can be simplified by rewriting it as a product of a Van der Monde determinant and exponentials. The determinant then reduces to a Van der Monde polynomial [46],

$$\det S\left(X_\alpha\right) = \prod_{i<j=1}^{N_\alpha} \left|x_i^\alpha - x_j^\alpha\right| \prod_{i=1}^{N_\alpha} e^{-\gamma\left(x_i^\alpha\right)^2},$$

where $\gamma = 1/2$ for single particle in a harmonic potential. Here it will be considered as a variational parameter in VMC. A different wavefunction was used by Carbonell-Coronado *et al.* [41] so the comparison with their results can be used as a test of the choice of the trial wavefunction.

4.2 Energy and Contact

Our goal in this section is to understand how the interplay between statistics and interaction affects the energetic properties of the system. We are going to use Tan's contact C, discussed in section 2.4, to estimate the interaction energy (2.11). Since Tan's contact is defined as a derivative of the enrgy with respect to the scattering length (2.10), I used finite difference to calculate it from the FN DMC energies as in [42]. The dependence of the contact C on the strength of the interaction is plotted in figure 1, using the same rescaling as in [42]. The results are normalized with respect to the total number of particles N. We can see that the number of components N_c is the most relevant parameter for this rescaled contact $C/N^{5/2}$, and the dependence on the number of particles in each component N_p is negligible. By increasing

the number of components, the absolute value of the rescaled contact grows. Even though the particles of each component obey Fermi-Dirac statistics, the entire system's behavior is similar to the system of N_c bosons (open symbols). These findings are consistent with the results from [42], which are shown with lines in figure 1. The lines are not perfectly smooth because the data were obtained by digitizing the figure from ref. [42].

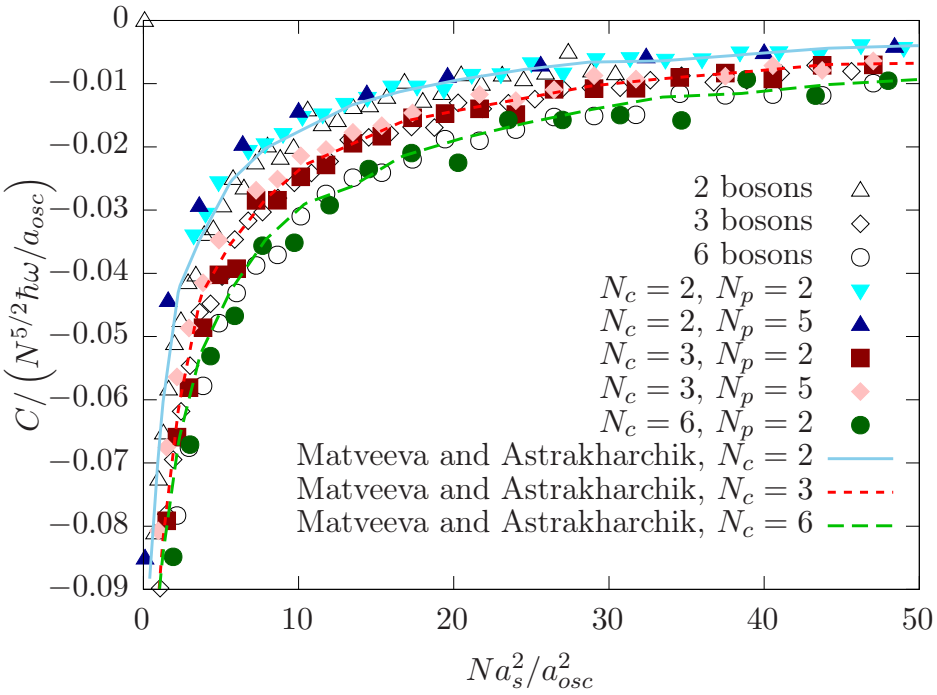

Figure 1: The contact C as a function of the interaction parameter Na_s^2/a_{osc}^2 for various balanced systems of N_c components with N_p particles each. The contact was obtained as a derivative (2.10) of FN-DMC energy. The lines are polynomial fits of the FN-DMC results by Matveeva and Astrakharchik [42]. Open black symbols are results of DMC for interacting bosons. The error bars are smaller than the symbol size.

The interaction energy, which is obtained from the contact as $E_{int} = -a_s C$, (shown in figure 2) also exhibits no significant dependence on N_p. Its value for fixed interaction strength is larger for larger number of components N_c. Again, the statistics of the particles in a component is irrelevant since the N_c-component Fermi system's behavior is similar to a system of N_c interacting bosons. The results match those from [42] (lines). Slight fluctuations around those lines (especially in the $N_c = 6$ case) are assumed to be statistical and are expected to disappear in a longer simulation. The inset shows the same function for higher interaction parameter Na_s^2. The data were fitted to a linear function which also matches the data for $N_c = 2$, $N_p = 5$.

Figure 3 shows the total energy E of a slightly imbalanced small system of $2+1$ particles as a function of the coupling constant g. The results accurately match those obtained by Carbonell-

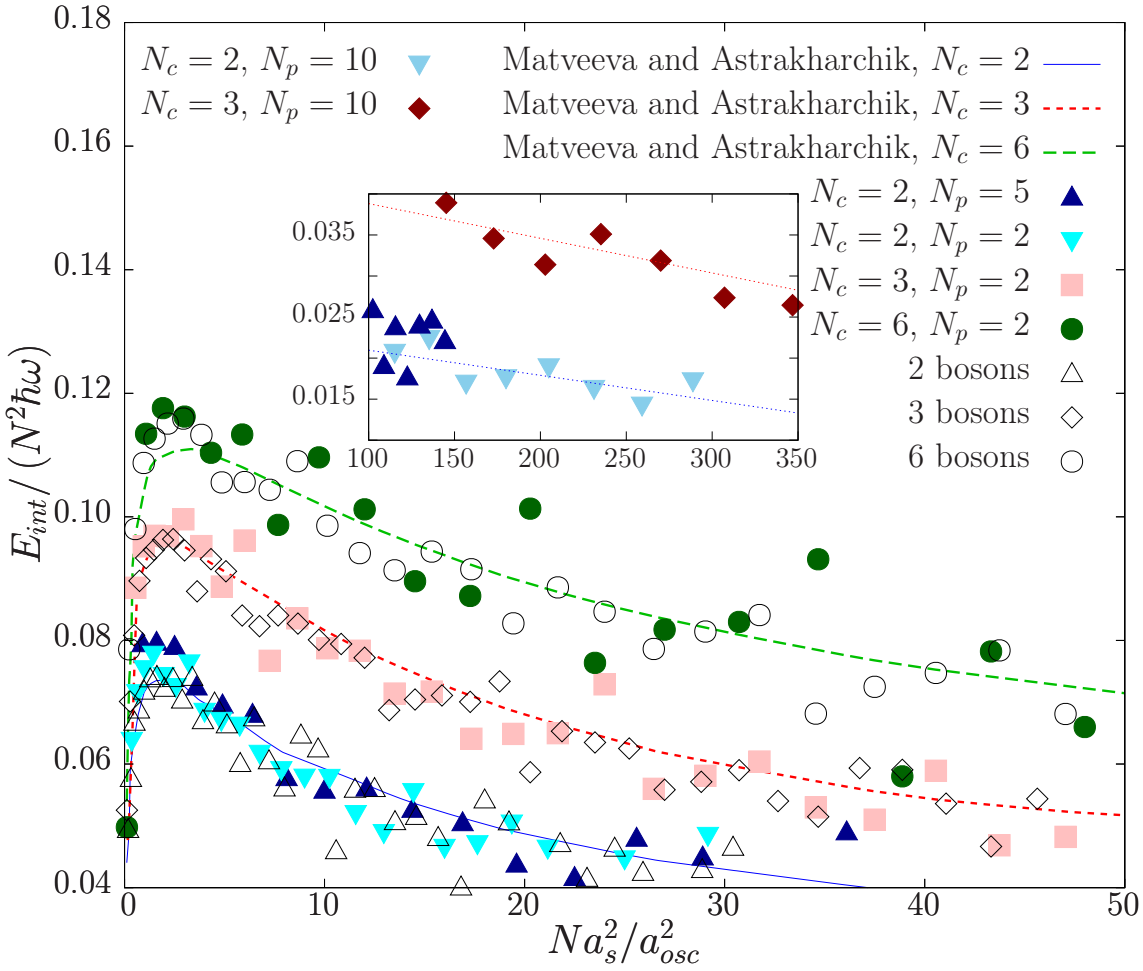

Figure 2: The interaction energy E_{int} as a function of the interaction parameter Na_s^2/a_{osc} for various balanced systems of N_c components with N_p particles each. The interaction energy was obtained as a function of the contact (2.11). The lines are polynomial fits of the FN-DMC results by Matveeva and Astrakharchik [42]. Open black symbols are DMC results for distinguishable bosons. The inset shows the same function for higher values of Na_s^2/a_{osc}, the lines are linear fits to FN-DMC data for the systems of 10 particles per component. The error bars are smaller than the symbol size.

Coronado *et al.* with FN-DMC using another trial wavefunction

$$\psi_{CC} = D^{\uparrow}D^{\downarrow}\prod_{i=1}^{N^{\uparrow}}\prod_{j=1}^{N^{\downarrow}}\phi\left(x_{ij}\right),$$

where $D^{\uparrow}, D^{\downarrow}$ are Slater determinants of the harmonic oscillator eigenfunctions for two components of fermions, $x_{ij} = |x_i - x_j|$ and

$$\phi\left(x_{ij}\right) = \begin{cases} \cos\left(k\left(x_{ij} - R_m\right)\right), & x_{ij} < R_m \\ 1, & x_{ij} \geq R_m \end{cases} \tag{4.3}$$

Here R_m is a variational parameter, and k is calculated for each value of a_s from the following

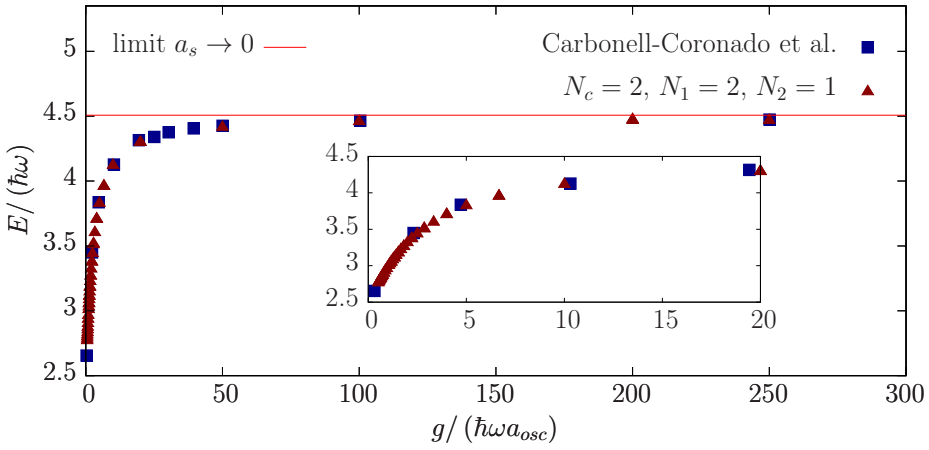

Figure 3: Total energy of the $2+1$ system as a function of the interaction strength g.
Red triangles represent the results of FN-DMC with $N_c = 2$, $N_1 = 2$, $N_2 = 1$. Blue squares are FN-DMC results from [41] for the same system. The red line is the energy in the limit of infinite repulsion. The inset is the same graph zoomed in.

transcendental equation

$$ka_s \tan(x_{ij} - R_m) = 1.$$

This is a confirmation of the choice that the trial wavefunction (4.2) did not affect the results. The same results are expected for any trial wavefunction with the same nodes as (4.2) and (4.3).

The total energy E of two-component balanced and slightly imbalanced systems is shown in figure 4 as a function of the total number of particles N. For comparison, the red shadowed rectangles indicate the interval of energies obtained by Carbonell-Coronado *et al.* [41] for the given number of particles N. There is a good correspondence between those results and my results (shown with points).

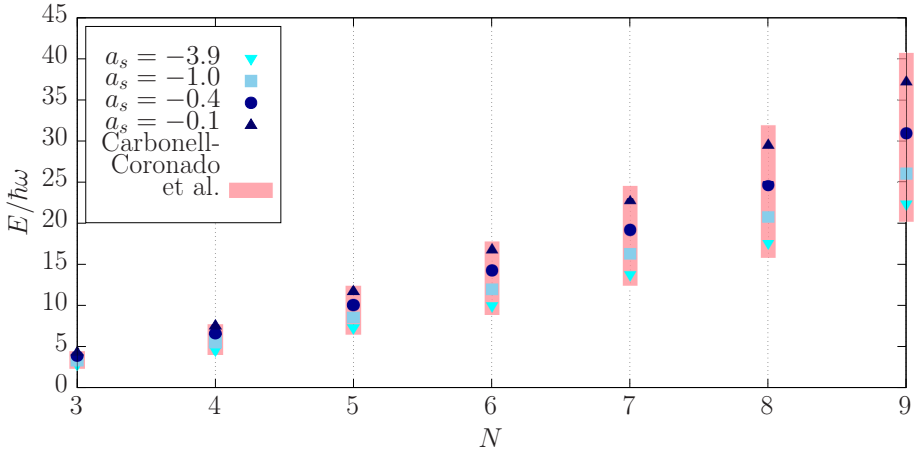

Figure 4: Total energy of two-component systems with 3-10 particles. The systems were either balanced $N/2$+$N/2$, for even N, or slightly imbalanced $(N+1)/2$+$(N-1)/2$, in the case of odd N. For fixed N, the energies are in the same interval as those obtained by Carbonell-Coronado *et al.* [41].

4.3 Density profile

Figure 5 shows density profile plots for balanced 4+4 and slightly imbalanced 4+5 two-component systems for three values of the interaction strength. The profiles are similar to those found in [41]. The distributions of the two components are alike for balanced systems and differ for the imbalanced ones. In the imbalanced case, the majority component particles tend to spread wider and get closer to the edge of the trap, at least in the parameter range given here. Also, the density distribution of the component with an even number of particles has a minimum in the center of the trap, while the component with an odd number of particles has a maximum there. In both balanced and imbalanced case, increasing repulsion strength causes the profiles to get wider.

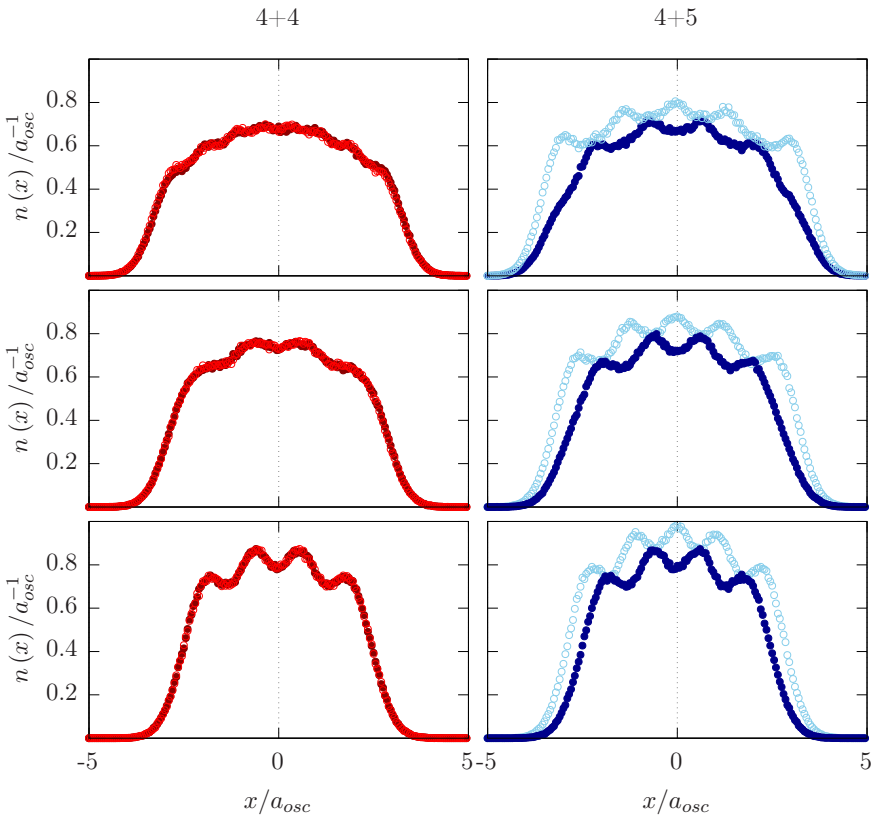

Figure 5: Separate component's density profiles for balanced 4+4 and slightly imbalanced 4+5 two-component systems with different interaction strengths. The balanced system is plotted in red on the left and the imbalanced is in blue on the right-hand side. The coupling constant is $g = 10$ in the top graphs, $g = 2.5$ in the middle and $g = 0.5$ in the bottom. The majority component density is plotted with light blue open circles and the minority component is plotted with dark blue solid circles. All profiles are normalized to the number of particles.

Figure 6 shows total density profiles of the same systems. Here it is more obvious that, in the balanced case, the weak interaction profile resembles the density profile of N_c ideal trapped fermions. Medium repulsion causes the density distrubution to lose its distinctive peaks but, as the coupling constant further grows, the strong interaction replicates the Pauli principle so the mixed system's profile looks like the profile of $N = N_p N_c$ ideal fermions. This is further analysed in figure 7.

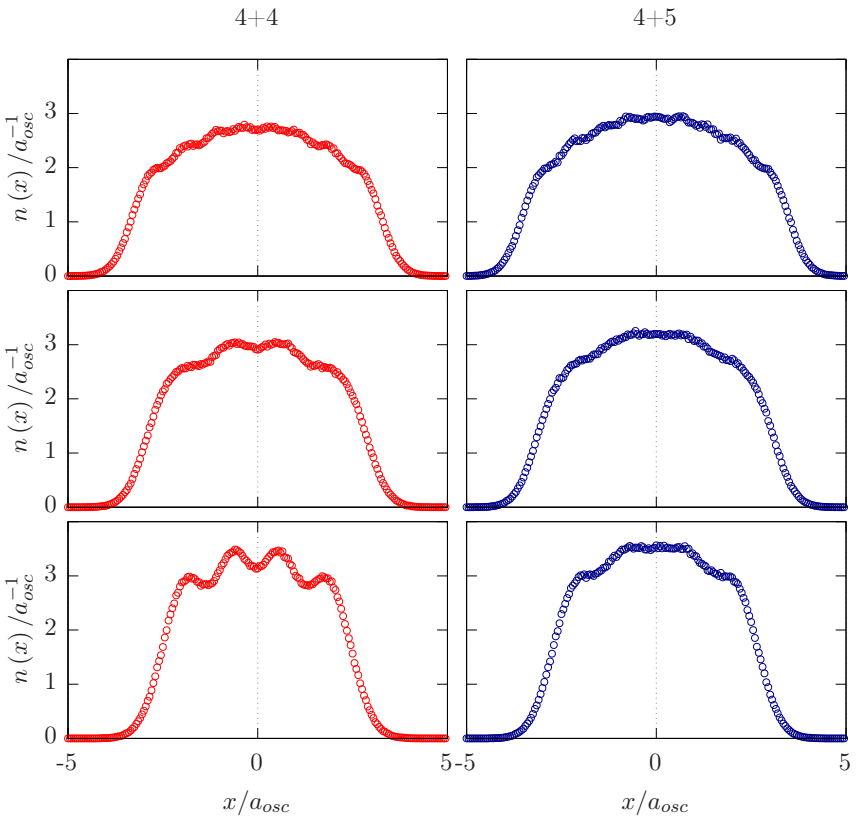

Figure 6: Total density profiles for balanced 4+4 and slightly imbalanced 4+5 two-component systems with different interaction strengths. The balanced system is plotted in red on the left and the imbalanced is in blue on the right-hand side. The coupling constant is $g = 10$ in the top graphs, $g = 2.5$ in the middle and $g = 0.5$ in the bottom. All profiles are normalized to the number of particles.

Desnity profiles for balanced two-component system with $N_p = 5$ are shown in figure 7. For weak repulsion ($g = 1$), the profile is similar to a density profile of 5 indistinguishable non-interacting trapped fermions (thin black line). As the coupling constant g grows, the profile gets wider and smoother, but as it grows even more ($g = 20$), new peaks become visible and the density approaches the density of 10 ideal fermions (thick black line).

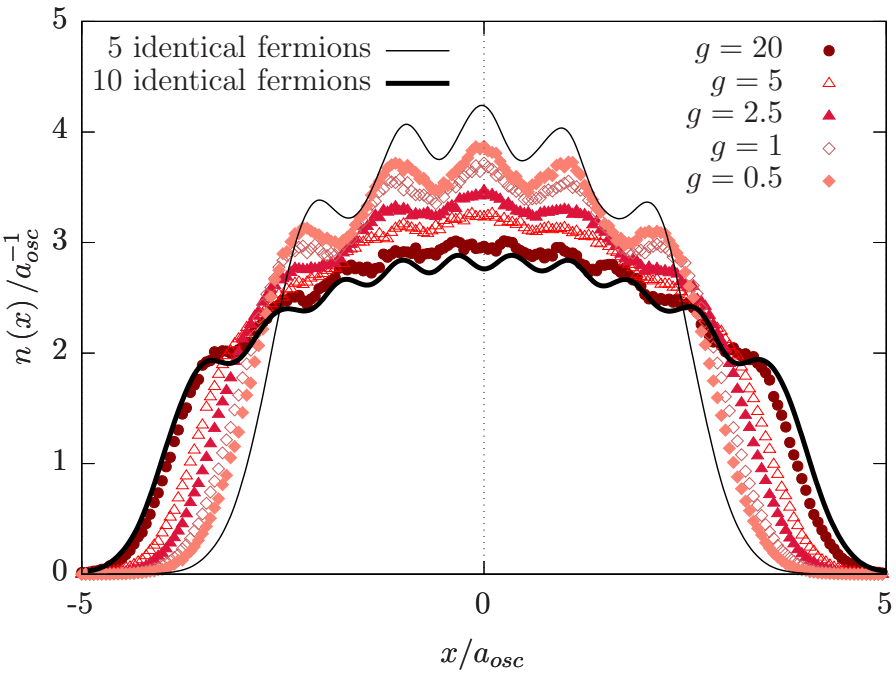

Figure 7: Density profiles for balanced 5+5 two-component system for different interaction strengths. The scattering lengths are listed in the top right corner and the corresponding coupling constants are: solid circles $g = 20$, open triangles $g = 5$, solid triangles $g = 2.5$, open squares $g = 1$, and solid squares $g = 0.5$. Density profiles of indistinguishable non-interacting trapped fermions are plotted with black lines, thin line corresponding to $N_p = 5$, thick line $N_p = 10$.

5 Bose - Fermi mixtures

Since the results for the Fermi mixtures agree well with the existing results [41, 42], we can now be confident in the method and continue to the new results. In this chapter, ground state properties of mixtures of Bose and Fermi particles will be studied using the FN-DMC method.

The Hamiltonian of the system will be the same as in the previous chapter (4.1) but since we are now dealing with bosons, the wavefunction will require some changes in order to ensure the right inter-component statistics so I start this chapter by introducing those changes. After that, the results will be given in the same order as in the previous chapter. First we will discuss the energy and Tan's contact. After that, some interesting density profiles will be shown in order to better understand the mixing of different types of particles.

5.1 Model Hamiltonian and trial wave function

The goal in this chapter is to obtain the ground state properties of balanced mixtures of N_c^B components of bosons and N_c^F components of fermions with N_p particles each, described by the balanced version of the Hamiltonian (4.1):

$$\hat{H} = -\frac{\hbar^2}{2m}\sum_{\alpha=1}^{N_c}\sum_{i=1}^{N_p}\partial_{\alpha i}^2 + g\sum_{\alpha<\beta=1}^{N_c}\sum_{i,j=1}^{N_p}\delta\left(x_i^\alpha - x_j^\beta\right) + \frac{m\omega^2}{2}\sum_{\alpha=1}^{N_c}\sum_{i=1}^{N_p}\left(x_i^\alpha\right)^2, \tag{5.1}$$

where $N_c = N_c^B + N_c^F$. All particles have the same mass m and scattering length a_s. The units defined in the previous chapter will be used: $\hbar\omega$ for energy, and a_{osc} for length.
Changes of the trial wavefunction (4.2) need to be made to take the Bose-Einstein statistics of the bosonic components into account. The total trial wavefunction will be taken to be separable into three functions: ψ_F for fermions, given with (4.2), ψ_B for bosons given with

$$\psi_B = \prod_{\alpha<\beta=1}^{N_c^B}\prod_{i=1}^{N_p}\prod_{j=1}^{N_p}\left|\left|x_i^\alpha - x_j^\beta\right| - a_s\right|\prod_{i=1}^{N_p} e^{-\gamma\left(x_i^\alpha\right)^2},$$

and ψ_{BF} describing the Bose-Fermi interaction

$$\psi_{BF} = \prod_{\alpha=1}^{N_c^F}\prod_{\beta=1}^{N_c^B}\prod_{i=1}^{N_p}\prod_{j=1}^{N_p}\left|\left|x_i^\alpha - x_j^\beta\right| - a_s\right|.$$

The total trial wavefunction of the mixture is $\psi = \psi_B\psi_F\psi_{BF}$. As in the previous chapter, the nodes of the ground state wavefunction exist because of the Pauli principle and are known in 1D so the FN-DMC results are assumed to be statistically exact.

In this chapter, two types of three-component Bose-Fermi mixtures will be considered. The first is a mixture of two Fermi and one Bose component described with the Hamiltonian (5.1)

with $N_c = 3$ ($N_c^F = 2$, $N_c^B = 1$). The other type also has two Fermi and one Bose component, but the bosons have intra-component δ-repulsion characterized with the same coupling constant g as the Bose-Fermi and the Fermi-Fermi inter-component interaction.[5] Even though the Hamiltonian (5.1) and the trial wavefunction $\psi = \psi_B\psi_F\psi_{BF}$ don't account for the intra-component Bose-Bose interaction, we can tweak the parameters a bit so we can still use these expressions. If we split the N_p-particle one component of bosons into N_p components with 1 particle each (keeping their mass and other properties unchanged), the intra-component repulsion would technically become inter-component repulsion described with ψ_B. This is exactly how this was done in the code. Although this is formally an imbalanced mixture of $N_c = 2+N_p$ components, described with (4.1) where $N_\alpha = 2$ and $N_\beta = N_p$, the bosons are still indistinguishable and I will regard it as a balanced three-component system.

For the remainder of this chapter, I will refer to the mixture with non-interacting bosons as *BF* and the mixture with interacting bosons as *BFi*.

5.2 Energy and Contact

In this section, I am going to explore the energetic properties of BF and BFi mixtures. In order to understand the role of statistics in 1D, all results will be compared with the results for Fermi mixtures from chapter 4.

Figure 8 shows the FN-DMC ground state energy E as a function of the total number of particles N for different scattering lengths a_s. Grey rectangles correspond to the energy range for a three-component Fermi mixture with the same number of particles. The BF mixture's energies (blue) are slightly lower than the plotted Fermi energy range, while the BFi mixture's energies (red) are close to BF results for weaker interaction and grow even higher then the Fermi mixture's energies as the scattering length gets lower ($a_s = -0.6$). Because of the different statistics, energy of non-interacting fermions is always higher than the energy of non-interacting bosons, so the difference between BF and Fermi mixtures' energies was expected. For strongly repulsive bosons in BFi system, interaction energy is large and the total energy becomes even higher than the ground state energy of the purely fermionic mixture.

Rescaled Tan's contact $C/N^{5/2}$ is plotted in figure 9 as a function of the interaction parameter Na_s^2. The results of BF (red) and BFi (blue) mixtures are compared with the results for Fermi mixtures from [42]. The BFi mixtures exibit behaviour similar to Fermi systems for low values of Na_s^2 (shown in the inset), while the BF mixtures' contacts have lower absolute values. For larger parameter Na_s^2, the interaction is weaker, so the interaction between the bosons in BFi contributes less. Consequentially, all observed three-component systems have simiar contact in this range of the interaction parameter.

[5] Adding fermionic intra-component contact repulsion wouldn't change the behavior of the system since the Fermi-Dirac statistics forbids the fermions to ever come into contact.

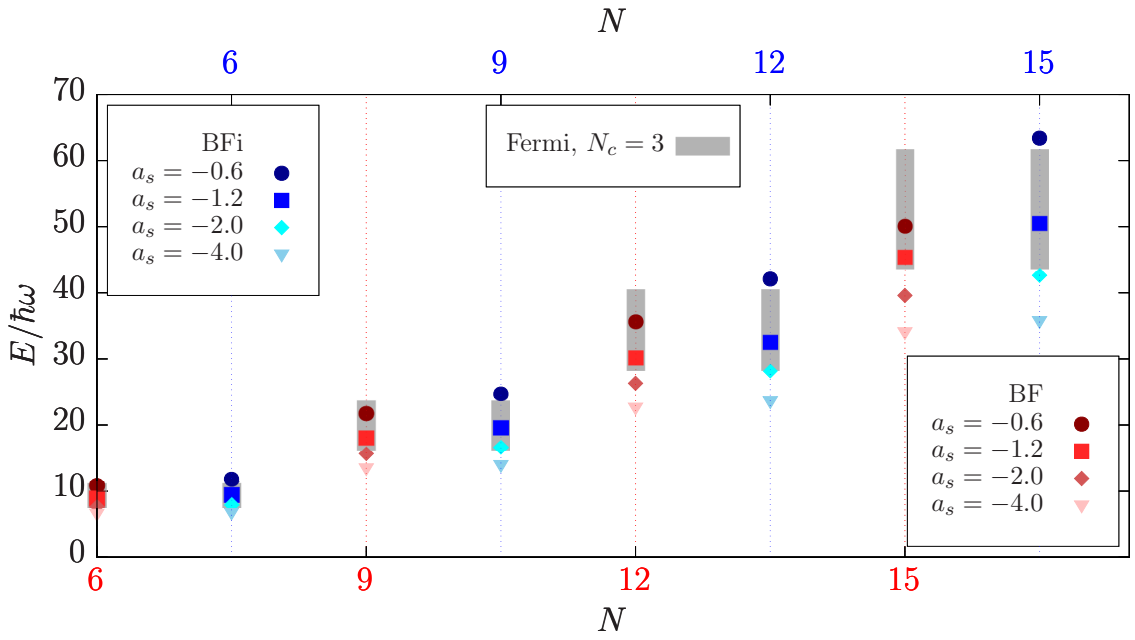

Figure 8: Total energy of three-component Bose-Fermi systems with 2-5 particles per component. Red symbols show FN-DMC ground state energies of BF systems, and blue sybmols show the energies of BFi systems. Grey rectangles are FN-DMC results for ground state energy of three-component Fermi mixtures for the same range of scattering length.

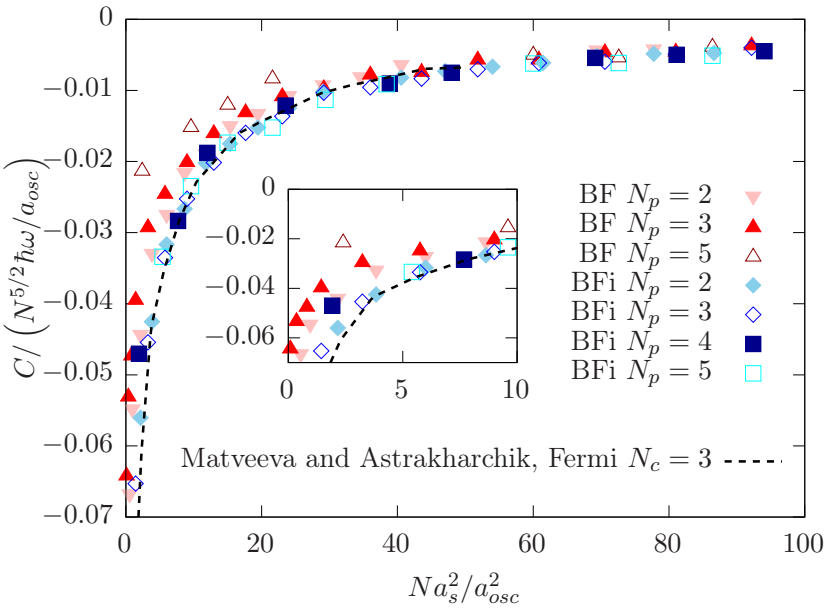

Figure 9: The contact C as a function of the interaction parameter Na_s^2/a_{osc}^2 for various 3-component systems. The contact was obtained as a derivative (2.10) of FN-DMC energy. The line is a polynomial fit of the FN-DMC results by Matveeva and Astrakharchik [42] for balanced three-component Fermi mixtures. Red triangles show FN-DMC results for Bose-Fermi-Fermi (BF) systems. The results for Bose-Fermi-Fermi systems with interacting Bose component (BFi) are plotted with blue squares. The inset is the same graph zoomed in. The errorbars are smaller than the symbol size.

Figure 10 shows the interaction energy E_{int}/N^2, given with (2.11), as a function of Na_s^2. The results are again compared with the interaction energy of three-component Fermi mixtures from [42]. The BFi energy exibits similar behavior as the purely fermionic mixtures, while the BF mixtures' results are slightly lower. This difference in the interaction energy is especially large in the range of low Na_s^2 (shown in the inset). This parameter range corresponds to strong repulsion and this is where the systems' nature differs the most. The interaction between bosons largely contributes to E_{int} which explains the different results for BF and BFi systems. The similarity between BFi and Fermi mixtures' interaction energies indicates that strong repulsion of bosons is mimicking the Pauli principle for fermions. Something similar is observed in the BFi mixtures' density profiles.

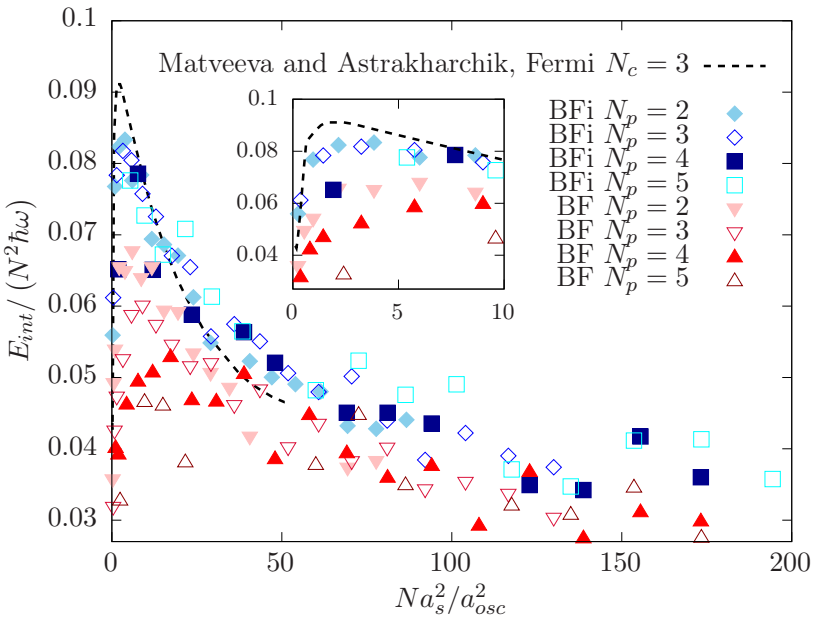

Figure 10: The interaction energy E_{int} as a function of the interaction parameter Na_s^2/a_{osc}^2 for various 3-component systems. The interaction energy was obtained as a function of the contact (2.11). The line is a polynomial fit of the FN-DMC results by Matveeva and Astrakharchik [42] for balanced three-component Fermi mixtures. Red triangles show FN-DMC results for Bose-Fermi-Fermi (BF) systems. The results for Bose-Fermi-Fermi systems with Bose-Bose intra-component repulsion (BFi) are plotted with blue squares. The inset is the same graph zoomed in. The errorbars are smaller than the symbol size.

5.3 Density profile

Figures 11, 12, 13 show density profiles $n(x)$ of BF (left) and BFi (right) systems with coupling constants $g = 0.5,\ 2.5,\ 25$, respectively, and up to 5 particles per component. Bosons are always in the middle, surrounded by fermions that tend to get closer to the edge of the trap as the repulsion becomes stronger.

In the BF case, since the bosons do not interact with each other, their profile always has only one central peak, regardless of the interaction strength. The interaction only affects its width - since the repulsion pushes the bosons away from the fermions, as the interaction grows, their profile gets narrower. As the coupling constant grows, the fermions get pushed away from the center of the trap. In the case of large g (figure 13), the competition between Pauli principle and strong repulsion becomes visible. The fermions are getting pushed to the edge of the trap by the bosons sitting in the center and the trap is pushing them back to the center. There is a strong repulsive interaction between the two types of fermions and the anti symmetry of the wavefunction of each component which results in separation of the different fermionic components. This transition from mixed (figure 11) to separated (figure 13) phase for the fermions in a 9-particle system happens for values of the coupling constant $g \in \langle 7.7, 9.1 \rangle$ (figure 14). Since the separation happens in the 9- and 15-particle systems, the same is expected for the 6-particle system but for larger values of the coupling constant g.

In the BFi case, the Bose component's profile depends on the coupling constant g. Weakly interacting system (figure 11) is similar to the corresponding BF mixture. Since there still is some repulsion between the bosons, their density profile is a bit wider then the BF one, but there is still only one peak. As the interaction grows stronger, the bosons' profile gets wider (figure 12). Strongly interacting (figure 13) bosons' profile has an odd shape. There are many shallow extrema along a triangular shaped profile. Both Fermi and Bose profiles are very wide and largely overlap. If we look at the profile of the whole system (plotted in grey), we can see that is very similar to the profile of $N = 3N_p$ ideal fermions (thick black line). Again, strongly repulsive 1D system is behaving similarly to a non-interacting system obeying Fermi-Dirac statistic.

The last two plots in figure 13, where $N_p = 5$, show the simulation results at this moment, and require further calculations. The profiles are expected to look similar to the $N_p = 3$ case after sufficiently long simulation time.

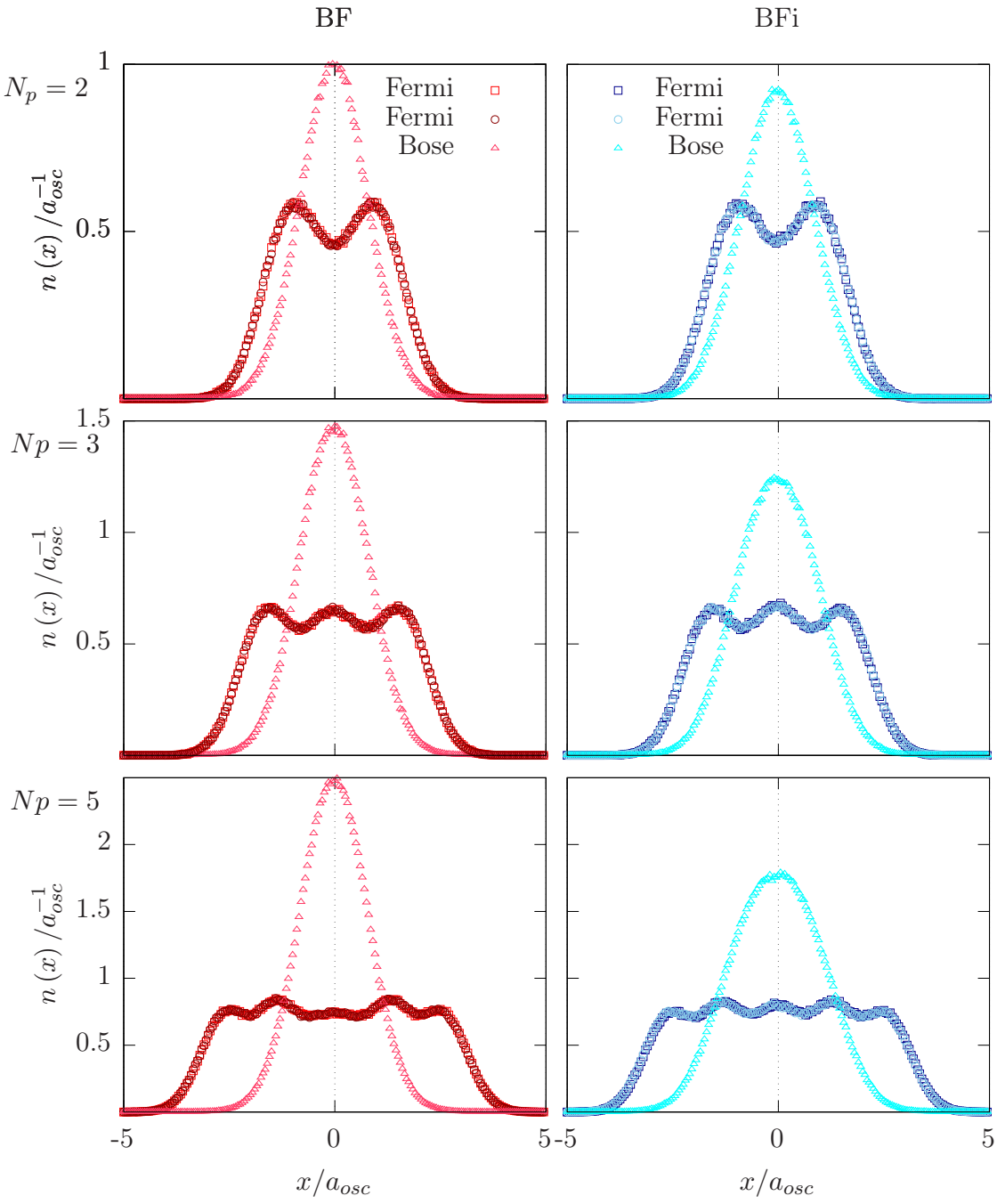

Figure 11: The density profiles for BF and BFi systems with up to 5 particles per component. The BF system is plotted on the left and BFi is on the right-hand side. The coupling constant is $g = 0.5$. All profiles are normalized to the number of particles.

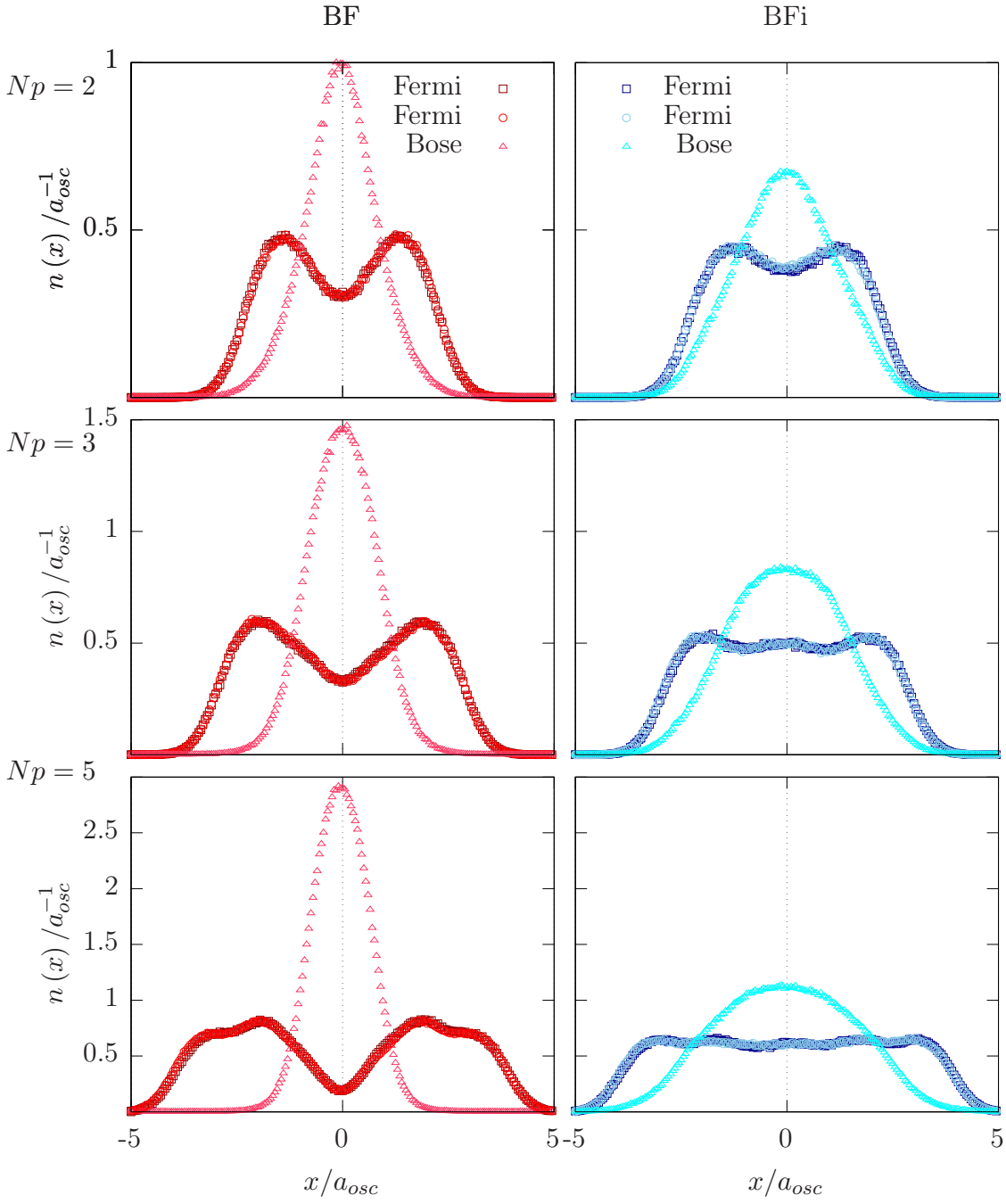

Figure 12: The density profiles for BF and BFi systems with up to 5 particles per component. The BF system is plotted on the left and BFi is on the right-hand side. The coupling constant is $g = 2.5$. All profiles are normalized to the number of particles.

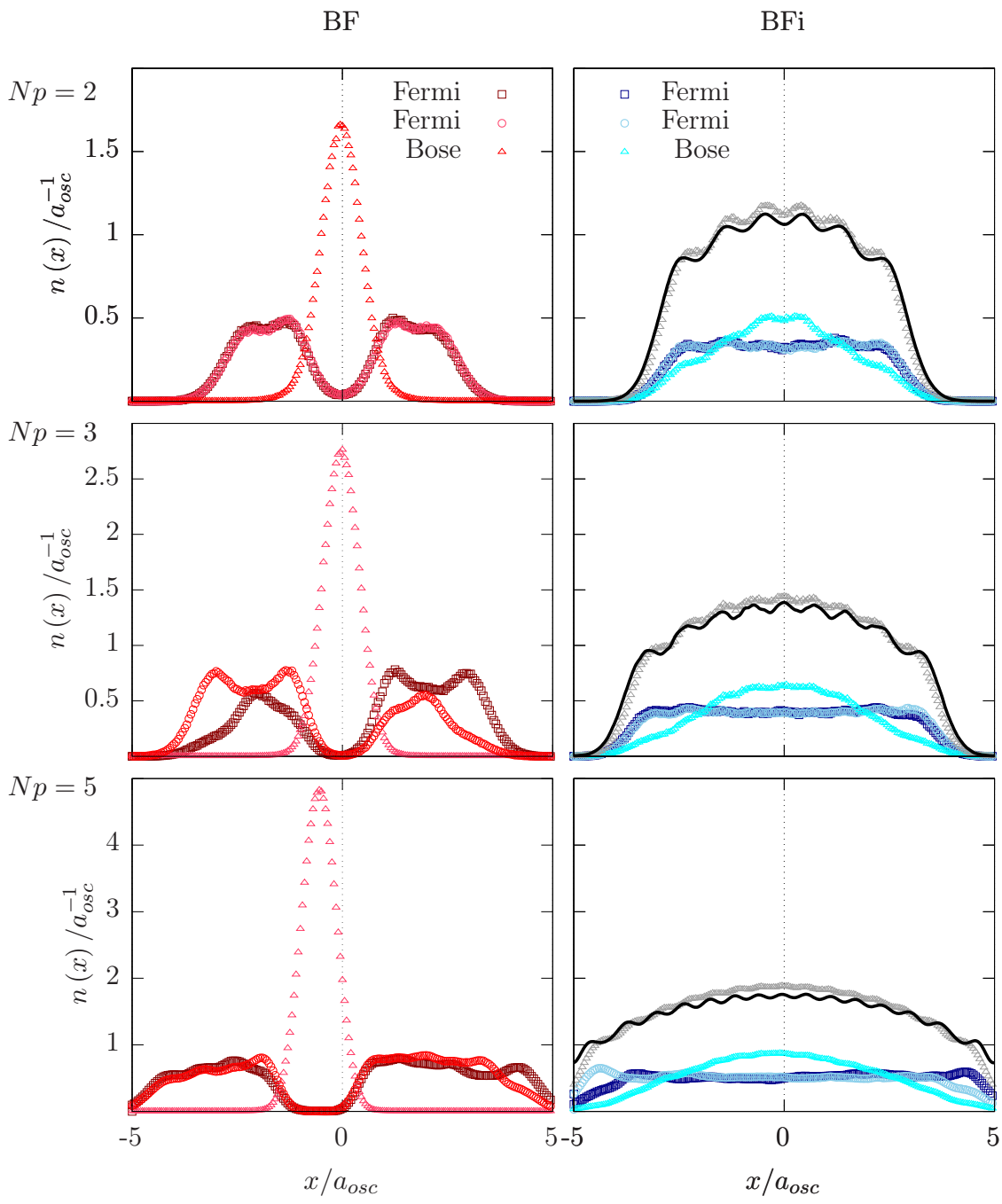

Figure 13: The density profiles for BF and BFi systems with up to 5 particles per component. The BF system is plotted on the left and BFi is on the right-hand side. Total density profile for the BFi systems is plotted with grey triangles. The black line is the density profile od $N = 3N_p$ identical non-interacting trapped fermions. The coupling constant is $g = 25$. All profiles are normalized to the number of particles.

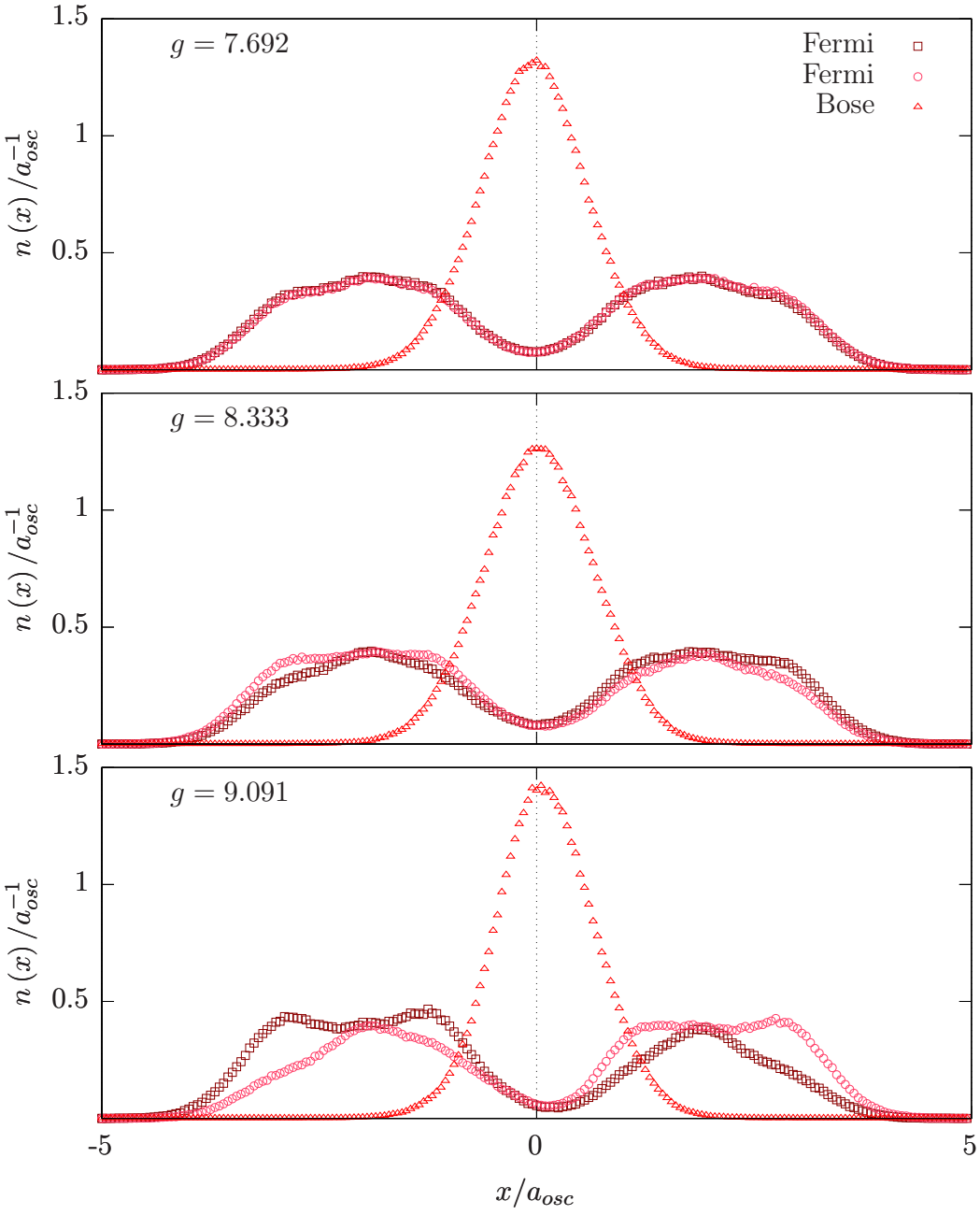

Figure 14: The transition from mixed to separated phase for BF system with 3 particles per component. The top profile show the system with coupling constant $g \approx 7.7$ in a mixed phase. By increasing the coupling constant, around $g \approx 8.3$, a transition starts (shown in the middle). The bottom density profile shows a separated system at $g \approx 9$.

6 Conclusion

To sum up, in this thesis I calculated ground state properties of two types of three-component Bose-Fermi mixtures with contact inter-species repulsion $g\delta(x_1 - x_2)$ trapped in an external harmonic potental. One type (BF) had no intra-component interaction and the other (BFi) had Bose-Bose intra-component contact repulsion characterized with the same coupling constant g as the inter-component interaction.

I used fixed node Monte Carlo method to obtain properties connected to ground state energies and density profiles of the systems of interest. The method was first tested on multi-component Fermi mixtures by comparison with existing results [41, 42]. I calculated the ground state energy as a function of the coupling constant for multi-component systems and used those results to find Tan's contact and the interaction energy. The results agree with those from [42]. Results for both balanced and imbalanced two-component Fermi systems match the data from [41].

The motivation for studying Bose-Fermi mixtures was to gain insight in the interplay of statistics and interaction that happens in one-dimensional systems. This is why the results were systematically compared with those for Fermi-Fermi mixtures with the same number of particles. I found that the energy of the BF systems is slightly lower than the energy of their fermionic counterparts, while the energy of BFi systems shows larger dependence on the coupling constant since the interaction energy contributes more to the system's ground state energy. The calculations of Tan's contact and the interaction energy confirmed this. The BFi systems were closer to Fermi mixtures than the BF mixtures.

The density profiles of Fermions in BF mixtures show a phase transition from mixed to a separated phase for strongly coupled systems. In both weakly and strongly interacting regimes, the non-interacting bosons sit in the middle of the trap while the fermions are closer to the edge. For weak and medium repulsion, the density profiles of the two fermionic components overlap. In the strongly coupled regime, their profiles separate so that the neighboring particles are of different species.

The BFi mixtures show similar behavior in the weakly interacting regime, but the separation does not happen. Both Bose and Fermi density profiles get wider as the repulsion gets stronger and, in the case of strong repulsion, the total system's profile has the shape of the density profile of N non-interacting identical fermions which indicates the fermionization of the system.

The research could be continued in various directions. Since I calculated Tan's contact, which is defined as a coefficient describing the high-momentum tail of the momentum distribution, continuing with calculations of the momentum distributions of BF and BFi systems is imposed as a logical next step. It could be interesting to see if the fermionization of the strongly interacting BFi systems happens in the momentum space. Since the contact of the BFi mixtures agrees

with the results for Fermi mixtures, similar momentum distributions are expected in the high-momentum limit, but the low-momentum range is expected to be governed with statistics since bosons usually have sharp peak around $k = 0$ and fermions tend to have wider low-momentum distributions.

7 Bibliography

[1] H. Bethe, "Zur theorie der metalle," Zeitschrift für Physik, vol. 71, pp. 205–226, Mar 1931.

[2] J. M. Thijssen, Computational Physics. Cambridge University Press, 2007.

[3] M. A. Cazalilla, R. Citro, T. Giamarchi, E. Orignac, and M. Rigol, "One dimensional bosons: From condensed matter systems to ultracold gases," Rev. Mod. Phys., vol. 83, pp. 1405–1466, Dec 2011.

[4] X.-W. Guan, M. T. Batchelor, and C. Lee, "Fermi gases in one dimension: From Bethe ansatz to experiments," Rev. Mod. Phys., vol. 85, pp. 1633–1691, Nov 2013.

[5] A. N. Wenz, G. Zürn, S. Murmann, I. Brouzos, T. Lompe, and S. Jochim, "From few to many: Observing the formation of a Fermi sea one atom at a time," Science, vol. 342, no. 6157, pp. 457–460, 2013.

[6] F. Serwane, G. Zürn, T. Lompe, T. B. Ottenstein, A. N. Wenz, and S. Jochim, "Deterministic preparation of a tunable few-fermion system," Science, vol. 332, no. 6027, pp. 336–338, 2011.

[7] G. Zürn, F. Serwane, T. Lompe, A. N. Wenz, M. G. Ries, J. E. Bohn, and S. Jochim, "Fermionization of two distinguishable fermions," Phys. Rev. Lett., vol. 108, p. 075303, Feb 2012.

[8] I. Bloch, J. Dalibard, and W. Zwerger, "Many-body physics with ultracold gases," Rev. Mod. Phys., vol. 80, pp. 885–964, Jul 2008.

[9] W. D. Phillips, "Nobel lecture: Laser cooling and trapping of neutral atoms," Rev. Mod. Phys., vol. 70, pp. 721–741, Jul 1998.

[10] G. Pagano, M. Mancini, G. Cappellini, P. Lombardi, F. Schäfer, H. Hu, X.-J. Liu, J. Catani, C. Sias, M. Inguscio, and L. Fallani, "A one-dimensional liquid of fermions with tunable spin," Nature Physics, vol. 10, pp. 198 EP –, Feb 2014.

[11] S. Murmann, F. Deuretzbacher, G. Zürn, J. Bjerlin, S. M. Reimann, L. Santos, T. Lompe, and S. Jochim, "Antiferromagnetic Heisenberg spin chain of a few cold atoms in a one-dimensional trap," Phys. Rev. Lett., vol. 115, p. 215301, Nov 2015.

[12] T. Kinoshita, T. Wenger, and D. S. Weiss, "Observation of a one-dimensional Tonks-Girardeau gas," Science, vol. 305, no. 5687, pp. 1125–1128, 2004.

[13] B. Paredes, A. Widera, V. Murg, O. Mandel, S. Fölling, I. Cirac, G. V. Shlyapnikov, T. W. Hänsch, and I. Bloch, "Tonks-Girardeau gas of ultracold atoms in an optical lattice," Nature, vol. 429, no. 6989, pp. 277–281, 2004.

[14] E. Haller, R. Hart, M. J. Mark, J. G. Danzl, L. Reichsöllner, M. Gustavsson, M. Dalmonte, G. Pupillo, and H.-C. Nägerl, "Pinning quantum phase transition for a Luttinger liquid of strongly interacting bosons," Nature, vol. 466, pp. 597 EP –, Jul 2010.

[15] E. K. Laird, Z.-Y. Shi, M. M. Parish, and J. Levinsen, "SU(N) fermions in a one-dimensional harmonic trap," Phys. Rev. A, vol. 96, p. 032701, Sep 2017.

[16] J. Decamp, J. Jünemann, M. Albert, M. Rizzi, A. Minguzzi, and P. Vignolo, "Strongly correlated one-dimensional Bose–Fermi quantum mixtures: Symmetry and correlations," New Journal of Physics, vol. 19, p. 125001, dec 2017.

[17] N. Zettili, Quantum Mechanics: Concepts and Applications. Wiley, 2009.

[18] G. Astrakharchik, Quantum Monte Carlo study of ultracold gases. PhD thesis, Dec 2014.

[19] A. Minguzzi, P. Vignolo, and M. Tosi, "High-momentum tail in the Tonks gas under harmonic confinement," Physics Letters A, vol. 294, no. 3, pp. 222 – 226, 2002.

[20] M. Olshanii and V. Dunjko, "Short-distance correlation properties of the Lieb-Liniger system and momentum distributions of trapped one-dimensional atomic gases," Phys. Rev. Lett., vol. 91, p. 090401, Aug 2003.

[21] S. Tan, "Energetics of a strongly correlated Fermi gas," Annals of Physics, vol. 323, pp. 2952–2970, Dec 2008.

[22] S. Tan, "Large momentum part of a strongly correlated Fermi gas," Annals of Physics, vol. 323, pp. 2971–2986, Dec 2008.

[23] S. Tan, "Generalized virial theorem and pressure relation for a strongly correlated Fermi gas," Annals of Physics, vol. 323, pp. 2987–2990, Dec 2008.

[24] M. Barth and W. Zwerger, "Tan relations in one dimension," Annals of Physics, vol. 326, no. 10, pp. 2544 – 2565, 2011.

[25] G. Lang, P. Vignolo, and A. Minguzzi, "Tan's contact of a harmonically trapped one-dimensional Bose gas: Strong-coupling expansion and conjectural approach at arbitrary interactions," European Physical Journal: Special Topics, vol. 226, pp. 1583–1591, May 2017.

[26] R. J. Fletcher, R. Lopes, J. Man, N. Navon, R. P. Smith, M. W. Zwierlein, and Z. Hadzibabic, "Two- and three-body contacts in the unitary Bose gas," Science, vol. 355, no. 6323, pp. 377–380, 2017.

[27] E. H. Lieb and W. Liniger, "Exact analysis of an interacting Bose gas. I. The general solution and the ground state," Phys. Rev., vol. 130, pp. 1605–1616, May 1963.

[28] E. H. Lieb, "Exact analysis of an interacting Bose gas. II. The excitation spectrum," Phys. Rev., vol. 130, pp. 1616–1624, May 1963.

[29] M. Girardeau, "Relationship between systems of impenetrable bosons and fermions in one dimension," Journal of Mathematical Physics, vol. 1, no. 6, pp. 516–523, 1960.

[30] V. Gurarie, "One-dimensional gas of bosons with Feshbach-resonant interactions," Phys. Rev. A, vol. 73, p. 033612, Mar 2006.

[31] F. Calogero, "Ground state of a one-dimensional N-body system," Journal of Mathematical Physics, vol. 10, no. 12, pp. 2197–2200, 1969.

[32] M. Brack and B. P. van Zyl, "Simple analytical particle and kinetic energy densities for a dilute fermionic gas in a d-dimensional harmonic trap," Phys. Rev. Lett., vol. 86, pp. 1574–1577, Feb 2001.

[33] T. C. Dorlas, "Orthogonality and completeness of the Bethe ansatz eigenstates of the non-linear Schroedinger model," Comm. Math. Phys., vol. 154, no. 2, pp. 347–376, 1993.

[34] G. Lang, Correlations in low-dimensional quantum gases. PhD thesis, 2017.

[35] C. N. Yang, "Some exact results for the many-body problem in one dimension with repulsive delta-function interaction," Phys. Rev. Lett., vol. 19, pp. 1312–1315, Dec 1967.

[36] M. Gaudin, "Un systeme a une dimension de fermions en interaction," Physics Letters A, vol. 24, no. 1, pp. 55 – 56, 1967.

[37] N. Metropolis, A. Rosenbluth, M. Rosenbluth, A. Teller, and E. Teller, "Equation of state calculations by fast computing machines," J. Chem. Phys., vol. 21, p. 1087, 1953.

[38] H. F. Trotter, "On the product of semi-groups of operators," Proceedings of the American Mathematical Society, vol. 10, no. 4, pp. 545–551, 1959.

[39] R. M. Wilcox, "Exponential operators and parameter differentiation in quantum physics," Journal of Mathematical Physics, vol. 8, no. 4, pp. 962–982, 1967.

[40] J. Boronat, "Monte Carlo simulations at zero temperature: Helium in one, two, and three dimensions," pp. 21–33, 12 2002.

[41] C. Carbonell-Coronado, F. D. Soto, and M. C. Gordillo, "Ordering in one-dimensional few-fermion clusters with repulsive interactions," New Journal of Physics, vol. 18, p. 025015, feb 2016.

[42] N. Matveeva and G. E. Astrakharchik, "One-dimensional multicomponent fermi gas in a trap: quantum monte carlo study," New Journal of Physics, vol. 18, p. 065009, jun 2016.

[43] C. Chin, R. Grimm, P. Julienne, and E. Tiesinga, "Feshbach resonances in ultracold gases," Review of Modern Physics, vol. 82, p. 1225, 04 2010.

[44] M. Olshanii, "Atomic scattering in the presence of an external confinement and a gas of impenetrable bosons," Physical Review Letters, vol. 81, 04 1998.

[45] G. E. Astrakharchik, "Local density approximation for a perturbative equation of state," Phys. Rev. A, vol. 72, p. 063620, Dec 2005.

[46] S. Karlin and G. Szegö, "On certain determinants whose elements are orthogonal polynomials," Journal d'Analyse Mathématique, vol. 8, pp. 1–157, Dec 1960.

A The Code

In section 3 we described the numerical methods used and later, in sections 4 and 5, the physical systems of interest were introduced and analyzed. Now that we have seen the results, one question still remains and that is how we implement the algorithms and the system. In this part I am going to go through the code[6] used in this thesis. I will try to avoid copying large chunks of the source and instead give pseudocode or, if possible, give graphical representations. The code was written in `C++` and is completely object-oriented so I will start with the class structure and then go through the most important functions and variables.

A.1 Class structure

The code is organized in two classes, shown in figure 15, class `Qsystem` and class `walker`.

- The class `walker` contains all the information on a walker, including its position in the phase space and functions for calculating and retrieving its energy, wavefunction and quantum force.
- The class `Qsystem` contains the algorithms for VMC and DMC, and all the information on a quantum system, including an array of `walker` objects used to describe it.

This division has many advantages. New algorithms may be later added without affecting the walkers or a new system can be implemented without changing the algorithms.
Further expansion of the code was planned and might be realized in the future. It would include a class `interaction` containing the system's wavefunction and potential, as well as the functions for calculating the associated local energy and quantum force. A `walker` object would then contain an `interaction` object and there would be no need to obtain analytic expressions of the local energy and drift force.

A.2 Walker

A `walker` object knows all the physical information about itself. Upon creation, it initializes its number of particles, their mass, spin, external potential frequency and scattering length by reading data from an `IN` file, show in figure 16. There is an option to change the dimensionality of the system `nd` but in was not used in this thesis since only 1D systems were explored. A walker also knows the positions of all of its particles, its wavefunction, local energy, and quantum force. They are calculated in functions `UpdatePsi()`, `UpdateEloc()`, `UpdateF()`

[6]The latest version of the code can be found on link https://github.com/gloriaodak/QMC.git

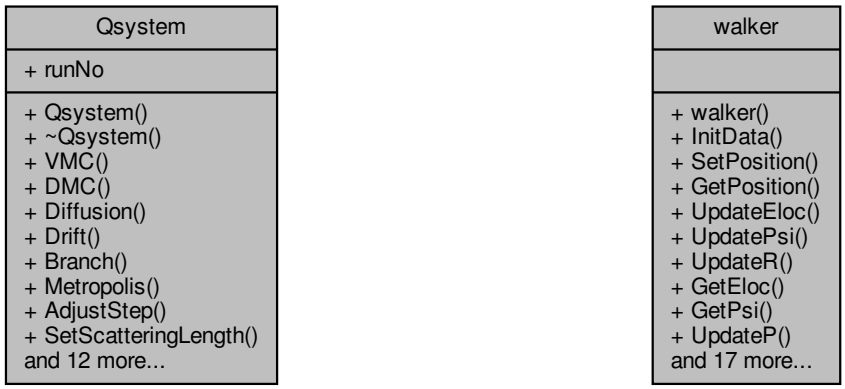

Figure 15: Class diagrams of classes `Qsystem` and `walker`

and this is the part of the code that needs to be changed when changing the physical system under observation. In this version, the energy and drift force need to be calculated beforehand using expressions (3.12), (3.11). For specific systems covered in this thesis, the trial wavefunction is given with (4.2) and the above-mentioned functions are listed in listings 1, 2 and 3, respectively.

Other than that, the class contains some functions whose purpose is purely technical such as `CleanUp()` which is used for deleting unnecessary pointers even before the walker's destruction is possible, increasing the program's efficiency and allowing the use of fewer resources.

Listing 1: The trial wavefunction example

```
void walker::UpdatePsi()
{
  Psi=1.0;
  int n=0, m=0;
  for(int ic=0; ic<nc; ic++)
  {
    for(int ip=0; ip<component[ic]; ip++)
    {
      for(int jp=0; jp<ip; jp++)
        Psi *= fabs( x[ip+n][0] - x[jp+n][0] );
      m=0;
      for(int jc=0; jc<ic; jc++)
      {
        for(int jp=0; jp<component[jc];jp++)
        Psi *= fabs( fabs( x[ip+n][0] - x[jp+m][0] ) - a[ip+n] );
        m+=component[jc];
      }
      Psi *= exp( -g *  x[ip+n][0] * x[ip+n][0]);
    }
    n+=component[ic];
  }
}
```

Listing 2: The local energy example

```
void walker::UpdateEloc()
{
double e,r;
Eloc=0;
int n=0;
int m=0;
for(int ic=0; ic<nc; ic++)
{
  for(int ip=0; ip<component[ic]; ip++)
  {
    e=2*g;
    for(int jp=0; jp<ip; jp++)
    {
      r=x[ip+n][0]-x[jp+n][0];
      e+=1/r/r;
    }
    for(int jp=ip+1; jp<component[ic]; jp++)
    {
      r=x[ip+n][0]-x[jp+n][0];
      e+=1/r/r;
    }
    m=0;
    for(int jc=0; jc<ic; jc++)
    {
      for(int jp=0; jp<component[jc]; jp++)
      {
        r=fabs(x[ip+n][0]-x[jp+m][0]);
        e+=1/(r-a[ip+n])/(r-a[ip+n]);
      }
      m+=component[jc];
    }
    m+=component[ic];
    for(int jc=ic+1; jc<nc; jc++)
    {
      for(int jp=0; jp<component[jc]; jp++)
      {
        r=fabs(x[ip+n][0]-x[jp+m][0]);
        e+=1/(r-a[ip+n])/(r-a[ip+n]);
      }
      m+=component[jc];
    }
    e-=F[ip+n][0]*F[ip+n][0]/4.0;
    e*=D[ip+n];
    Eloc+=e;
    Eloc+=ho[ip+n]*x[ip+n][0]*x[ip+n][0];
  }
  n+=component[ic];
}
}
```

Listing 3: The drift force example

```
void walker::UpdateF()
{
int n=0;
int m=0;

for(int ic=0; ic<nc; ic++)
{
  for(int ip=0; ip<component[ic]; ip++)
  {

    F[ip+n][0] = -2*g*x[ip+n][0];

    for(int jp=0; jp<ip; jp++)
      F[ip+n][0] += 1/( x[ip+n][0] - x[jp+n
    ][0] );

    for(int jp=ip+1; jp<component[ic]; jp++)
      F[ip+n][0] += 1/( x[ip+n][0] - x[jp+n
    ][0] );

    m=0;

    for(int jc=0; jc<ic; jc++)
    {
      for(int jp=0; jp<component[jc]; jp++)
      {
        double r = x[ip+n][0]-x[jp+m][0];
        F[ip+n][0] += (r-a[ip+n]*r/fabs(r))/(
    fabs(r)-a[ip+n])/(fabs(r)-a[ip+n]);
      }
      m+=component[jc];
    }
    m+=component[ic];

    for(int jc=ic+1; jc<nc; jc++)
    {
      for(int jp=0; jp<component[jc]; jp++)
      {
        double r = x[ip+n][0]-x[jp+m][0];
        F[ip+n][0] += (r-a[ip+n]*r/fabs(r))/(
    fabs(r)-a[ip+n])/(fabs(r)-a[ip+n]);
      }
      m+=component[jc];
    }
    F[ip+n][0]*=2;
  }
  n+=component[ic];
}
}
```

```
3
2       1.0     1.0     1       -0.04
1       1.0     1.0     -1      -0.04



_________________________________________________________________________________________________
................................INPUT FORMAT.....................................................
_________________________________________________________________________________________________
.       N       = total # particles                                                             .
.       N1      = # type 1 particles    mass    frequency       spin    scattering length       .
.       N2      = # type 2 particles    mass    frequency       spin    scattering length       .
.       N3      = # type 3 particles    mass    frequency       spin    scattering length       .
.       .                               .       .               .       .                       .
.       .                               .       .               .       .                       .
.       .                               .       .               .       .                       .
.       Nn      = # type n particles    mass    frequency       spin    scattering length       .
.                                                                                               .
.                                                                                               .
.       !!!!!!!!!!!!!!!!!!!!!!!!!!!!!!!!!!!!!!!!!!!!!!!!!!!!!!!!!!!!!!!!!!!!!!!!!!!!!!!!       .
.                               N = N1 + N2 + N3 + ... + Nn                                     .
.       !!!!!!!!!!!!!!!!!!!!!!!!!!!!!!!!!!!!!!!!!!!!!!!!!!!!!!!!!!!!!!!!!!!!!!!!!!!!!!!!       .
_________________________________________________________________________________________________


spin:
                0               boson
               -1               spin down fermion
                1               spin up fermion
```

Figure 16: A typical `IN` file. In this example, the system contains three particles, two spin up fermions and one spin down fermion. All particles have the same mass and feel the same external potential.

A.3 QSystem

A `Qsystem` object represents the quantum system under observation and its most important variable is an array of walker objects described in the previous section. Its core functions are `VMC` and `DMC`, along with some helper functions to clean up the code and make it readable.

A.3.1 VMC

The call graph for function VMC is shown in figure 17. It uses `walker` class functions for manipulating `walker` objects and `Qsystem` class functions, `Qsystem::Metropolis` being the most interesting one. The theory behind Metropolis and VMC was described in section 3, the implementation is straightforward and the pseudocodes of `Qsystem::VMC` and `Qsystem::Metropolis` functions are given in algorithms 2 and 1, respectively.

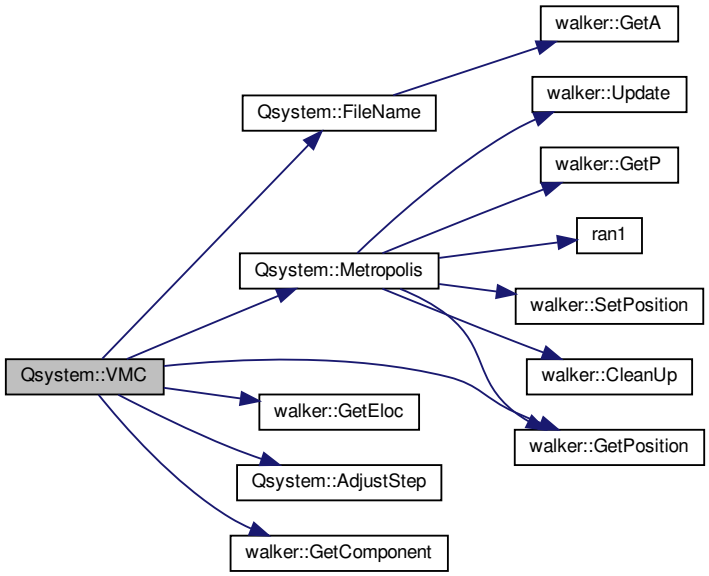

Figure 17: Call graph for function `VMC` of class `Qsystem`

Algorithm 1 a step s in the Metropolis algorithm

start with initial state $X_s = (x_1, \ldots, x_N)$
copy initial configuration to a temporary walker $X' = X_s$
generate random move dx in the interval $[-\delta, \delta]$
move one particle resulting in a state $X' = (x_1, \ldots, x'_i, \ldots, x_N)$
calculate transition probability $T(X_s \to X') = min\left\{\frac{\psi*(X')\psi(X')}{\psi*(X_s)\psi(X_s)}, 1\right\}$
if $T \geq 1$ **then**
  accept new configuration $X_{s+1} = X'$
else
  generate a random number r according to the uniform distribution
  if $r \leq \omega$ **then**
    accept new configuration $X_{s+1} = X'$
  else
    reject new configuration $X_{s+1} = X_s$
  end if
end if

Algorithm 2 Variational Monte Carlo

for every block **do**
  `SsE=0`
  for every step **do**
    `SwE=0`
    for all walkers **do**
      Metropolis (algorithm 1)
      accumulate energy `SwE+=`E_L and other estimators
    end for
    if block index > number of blocks to skip **then**
      accumulate energy `SsE+=`E_L and other estimators
    end if
  end for
  print averages of the energy and other estimators
  accumulate histograms
  adjust acceptance rate (listing 4)
end for
print histograms

Listing 4: The adustment of the acceptance rate

```
void Qsystem::AdjustStep(double acc)
{
  if(acc>0.5) for(int k=0; k<nd; k++) {maxStep[k] *= 1.05;}
  if(acc<0.5) for(int k=0; k<nd; k++) {maxStep[k] *= 0.95;}
}
```

A.3.2 DMC

The pseudocode of the DMC method, described in section 3.5, is given in algorithm 3. The implementation of this method is a bit more involved since it includes changing the size od the walker array. The walker array is defined in the constructor of class `Qsystem` as an array of `walker` objects of size `ncrit × 2`, where `ncrit` is a critical number of walkers around which the number of walkers `nw` will fluctuate during the simulation. This number is controlled in the function `Qsystem::branch()` given in listing 6. Every DMC step loops through the entire walker array, as described in the pseudocode, calculating energies and branching the array by destroying or creating copies of the existing walkers - *sons*. The number of sons `nSons` is calculated in the branching function `Qsystem::branch()`. Since this function may be difficult to understand, I will now try to explain it in more detail.
If a walkers has `nSons > 1`, then `nSons` of its copies are added to the end of the walker array (listing 9). It is important to note that now the array contains new walkers that are not

going to be looped through during this step, i.e. even though the size of the walker array has actually changed, the for loop's limit is kept at the old number of walkers.
If `nSons = 1`, no copies are made and the walker is kept on the same position in the array.
Finally, if the number of a walker's sons is zero, the walker will be deleted from the walker array. This is done in two steps: first the walker is *killed* using the function `walker::Die()` which sets the `walker` class variable `IsAlive` to false. Then, after looping through the entire walker array, the dead walkers are removed in the function `Qsystem::BuryDeadWalkers()` given in the listing 8. This function loops through the walker array looking for *dead* walkers. When it finds one, it moves the last *live* walker to its place, lowering the total number of walkers by one. After that, the number of walkers is redefined and used for looping through the array in the next step.

Algorithm 3 Diffusion Monte Carlo

for every block **do**
  reset energy `SsE = 0`
  for every step **do**
    reset energy `SwE = 0`
    reset number of dead walkers `nwDead = 0`
    define new number of walkers `nwNew = nw`
    for every walker, `iw = 0` $\rightarrow$ `nw` **do**
      if walker alive **then**
        save current walker's energy E_{old}= E
        copy current walker's configuration to `walker tmp`
        perform diffusion (listing 5) on `walker tmp`
        perform drift (listing 7) on `walker tmp`
        save energy of `walker tmp` to variable `E`
        perform branching (listing 6) on `walker tmp`
        accumulate energy `SwE += nSons` $\times$ `E` and other estimators
        define new number of walkers N_w^{new} += nSons -1
        if `nSons=0` **then**
          `nwDead++`
        end if
      end if
    end for
    remove dead walkers from the walker array (listing 8)
    redefine number of walkers `nw = nwNew`
    accumulate energy `SsE+=SwE` and other estimators
    adjust referent energy E_R
  end for
  accumulate energy `SbE+=SsE` and other estimators
  calculate averages
  print averages of the energy and other estimators
  accumulate histograms
end for
print histograms

Listing 5: The diffusion part of DMC

```
void Qsystem::Diffusion()
{
  double x,dx;
  double D;
  for(int ip=0; ip<np; ip++)
  {
    D=tmp.GetD(ip);
    for(int k = 0; k < nd; k++)
    {
      dx=var(D)*gasdev(&idum);
      x=tmp.GetPosition(ip,k);
      tmp.SetPosition(ip,k,x+dx);
    }
  }
}
```

Listing 6: The branching part of DMC

```
int Qsystem::Branch(int * iw, double Eold,
    double E)
{
  w=exp(tau * (Et -0.5*(E+Eold)));

  double r = ran1(&idum);
  nSons = (int)(w+r);

  if(nSons>0)
  {
    walkers[*iw]=tmp;
    if(nw>nwmax)
      nSons = (int)(nSons*reduce+ran1(&idum));
    else if(nw<nwmin)
      nSons = (int)(nSons*amplify+ran1(&idum))
    ;

    if (nSons>1)
    {
      CopyWalker(*iw,nSons);
      return nSons;
    }
    if(nSons==1)
      return nSons;

  }
  nSons=0;
  walkers[*iw].Die();
  return nSons;
}
```

Listing 7: The dirft part of DMC

```
double Qsystem::Drift()
{
  double **F1, **F2, x, **xold, dx*;
  double Eloc;
  double * D = new double [np];
  F1=new double * [np];
  F2=new double * [np];
  xold=new double * [np];

  for(int ip=0; ip<np; ip++)
  {
    F1[ip]=new double[nd];
    F2[ip]=new double[nd];
    xold[ip]=new double[nd];
    D[ip]=tmp.GetD(ip);

    for(int k=0; k<nd; k++)
    {
      F1[ip][k]=tmp.GetF(ip,k);
      x=tmp.GetPosition(ip,k);
      dx=D[ip]*0.5*tau*F1[ip][k];
      xold[ip][k]=x;
      tmp.SetPosition(ip,k,x+dx);
    }
  }

  tmp.Update();
  for(int ip=0; ip<np; ip++)
    for(int k=0; k<nd; k++)
      F2[ip][k]=tmp.GetF(ip,k);

  for(int ip=0; ip<np; ip++)
    for(int k=0; k<nd; k++)
    {
      dx=D[ip]*0.25*tau*(F1[ip][k]+F2[ip][k]);
      x=xold[ip][k];
      tmp.SetPosition(ip,k,x+dx);
    }

  tmp.Update();
  for(int ip=0; ip<np; ip++)
    for(int k=0; k<nd; k++)
      F1[ip][k]=tmp.GetF(ip,k);
  Eloc=tmp.GetEloc();

  for(int ip=0; ip<np; ip++)
    for(int k=0; k<nd; k++)
    {
      dx=D[ip]*tau*F1[ip][k];
      x=xold[ip][k];
      tmp.SetPosition(ip,k,x+dx);
    }

  for(int ip=0;ip<np;ip++)
  {
    delete [] F1[ip];
    delete [] F2[ip];
    delete [] xold[ip];
  }
  delete [] F1:
  delete [] F2;
  delete [] D;
  delete [] xold;
  return Eloc;

}
```

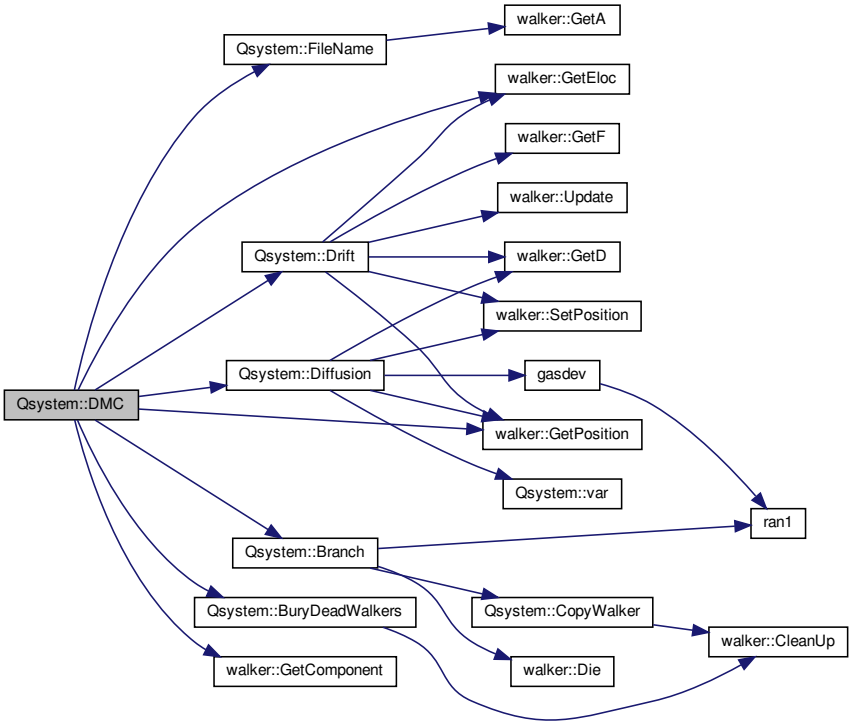

Figure 18: Call graph for function `DMC` of class `Qsystem`

Listing 8: Removing dead walkers from the walker array

```
void Qsystem::BuryDeadWalkers()
{
  walker copy;
  int N=nwNew+nwDead;
  for(int iw=0; iw<N && nwDead>0; iw++)
  {
    if(!walkers[iw].IsAlive())
    {
      while(!walkers[N-1].IsAlive())
      {
        nwDead--;
        N--;
      }
      if(iw<N-1)
      {
        copy = walkers[N-1];
        walkers[iw] = copy;
        N--;
        nwDead--;
      }
    }
  }
  copy.CleanUp();
}
```

Listing 9: Making copies of a walker and saving them at the end of the walker array

```
void Qsystem::CopyWalker(int iw, int n)
{
  walker copy;
  copy = walkers[iw];

  int N=nwNew+nwDead;

  for(int i=0;i<n-1;i++)
    walkers[N+i]=copy;

  copy.CleanUp();
}
```